Langmuir
Article
pubs.acs.org/Langmuir

Sorption of Aqueous Zn[II] and Cd[II] by Multiwall Carbon Nanotubes: The Relative Roles of Oxygen-Containing Functional Groups and Graphenic Carbon

Hyun-Hee Cho,[†] Kevin Wepasnick,[‡] Billy A. Smith,[‡] Fazlullah K. Bangash,[§] D. Howard Fairbrother,[‡] and William P. Ball*,[†]

[†]*Department of Geography and Environmental Engineering and* [‡]*Department of Chemistry, Johns Hopkins University, 3400 North Charles Street, Baltimore, Maryland 21218, and* [§]*Institute for Chemical Science, University of Peshawar, Peshawar 25120, Pakistan*

Received July 7, 2009. Revised Manuscript Received September 28, 2009

Exposure of multiwalled carbon nanotubes (MWCNTs) to oxidizing acids and other oxidants introduces oxygen-containing functional groups such as hydroxyl, carboxyl, and carbonyl groups onto the surface. This research evaluated how changes in oxygen concentration and distribution of oxygen-containing functional groups influenced the sorption of aqueous zinc and cadmium on MWCNTs. Sorption results with natural char, activated carbon, and a suite of MWCNTs (of varying surface oxygen content) were obtained. Results confirmed that surface oxygen enhances the sorption of both Zn[II] and Cd[II] from aqueous solution. Although Zn[II] sorbed more strongly than Cd[II] for all materials studied, surface oxidation had more effect on the sorption of Cd[II] than of Zn[II]. Additional sorption experiments with Zn[II] and 16 MWCNTs of varying surface oxidation level and functional group distribution revealed the relative contributions of different types of surface sites to sorption. Sorption isotherms were fit using a two-site Langmuir adsorption model that incorporated the independent characterization of functional group distribution. Results showed that carboxyl-carbon sites were over 20 times more energetic for zinc sorption than unoxidized carbon (graphenic-carbon) sites, though both site types are important contributors to sorption.

1. Introduction

Common aquatic contaminants include aluminum, chromium, magnesium, iron, cobalt, nickel, copper, zinc, cadmium, mercury, and lead.[1] The fate of these and other heavy metals in aquatic environments (e.g., surface water and groundwater) and in engineered processes (e.g., water and wastewater treatment) is largely controlled by their tendency to accumulate (adsorb) at solid−water interfaces.[2] Such adsorption can either retard the aquatic transport of the metals (e.g., through association with aquifer solids or sediments in natural systems or by fixation onto immobilized synthetic sorbents during water treatment) or facilitate their transport if the metals adsorb to mobile colloids. Within this context, carbonaceous materials are well-known to effectively adsorb many heavy metals, including Zn^{2+} and Cd^{2+},[3−5] and several past investigations have shown that acidic treatments of such materials will introduce surface oxygen that enhances the adsorption of metal cations.[6−14] Less is known, however, about metal sorption onto carbon nanotubes (CNTs), the focus of our current work. A second important motivation for this work is that the comparatively simple physical and chemical composition of CNTs (relative to activated carbon or naturally occurring carbonaceous sorbents) makes these materials an excellent substrate for conducting a mechanistic study of sorption affinities and capacities with different carbon-based surface functional groups.

A CNT consists of one (single-walled, SWCNT) or more (multiwalled, MWCNT) graphene sheets rolled into a cylinder[15] with an outer diameter in the range of 1−30 nm, thus creating a carbonaceous particle of extremely high aspect ratio and very high surface area per unit weight.[16,17] CNTs' high surface area to weight ratios make them strong sorbents for a wide variety of aqueous contaminants, including heavy metals such as cadmium,[18,19] zinc,[20,21] copper,[19] lead,[19,22] nickel,[23,24] and chromium,[25]

*Corresponding author. Telephone: 410-516-5434. Fax: 410-516-8996. E-mail: bball@jhu.edu.

(1) IPCS, International Programme on Chemical Safety. *Environmental Health Criteria*; World Health Organization: Geneva, 1988.
(2) Stumm, W.; Morgan, J. J. Kinetics at the solid-water interface. In *Aquatic chemistry: chemical equilibria and rates in natural waters*; Schnoor, J. L., Zehnder, A., Eds.; John Wiley & Sons, Inc.: New York, 1996.
(3) Gabaldon, C.; Marzal, P.; Ferrer, J.; Seco, A. *Water Res.* **1996**, *30*, 3050.
(4) Mohan, D.; Chander, S. *Colloids Surf.* **2001**, *177*, 183.
(5) Leyva Romos, R.; Bernal Jacome, L. A.; Mendoza Barron, J.; Fuentes Rubio, L.; Guerrero Coronado., R. M. *J. Hazard. Mater.* **2002**, *90*, 27.
(6) Chen, J. P.; Wu, S. *Langmuir* **2004**, *20*, 2233.
(7) Jia, Y. F.; Thomas, K. M. *Langmuir* **2000**, *16*, 1114.
(8) Aggarwal, D.; Goyal, M.; Bansal, R. C. *Carbon* **1999**, *37*, 1989.
(9) Rivera-Utrilla, J.; Sanchez-Polo, M. *Water Res.* **2003**, *37*, 3335.
(10) Machida, M.; Kikuchi, Y.; Aikawa, M.; Tatsumoto, H. *Colloids Surf., A* **2004**, *240*, 179.
(11) Machida, M.; Mochimaru, T.; Tatsumoto, H. *Carbon* **2006**, *44*, 2681.
(12) Sanchez-Polo, M.; Rivera-Utrilla, J. *Environ. Sci. Technol.* **2002**, *36*, 3850.
(13) Xiao, B.; Thomas, K. M. *Langmuir* **2005**, *21*, 3892.
(14) Shim, J. W.; Park, S. J.; Ryu, S. K. *Carbon* **2001**, *39*, 1635.
(15) Iijima, S. *Nature* **1991**, *354*, 56.
(16) Gibson, J. M.; Ebbensen, T. W.; Treacy, M. M. J. *Nature* **1996**, *381*, 678.
(17) Ebbesen, T. W.; Lezec, H. J.; Hiura, H.; Bennett, J. W.; Ghaemi, H. F.; Thio, T. *Nature* **1996**, *382*, 54.
(18) Li, Y.-H.; Wang, S.; Luan, Z.; Ding, J.; Xu, C.; Wu, D. *Carbon* **2003**, *41*, 1057.
(19) Li, Y. H.; Ding, J.; Luan, Z. K.; Di, Z. C.; Zhu, Y. F.; Xu, C. L.; Wu, D. H.; Wei, B. Q. *Carbon* **2003**, *41*, 2787.
(20) Lu, C.; Chiu, H.; Liu, C. *Ind. Eng. Chem. Res.* **2006**, *45*, 2850.
(21) Lu, C.; Chiu, H. *Chem. Eng. Sci.* **2006**, *61*, 1138.
(22) Wang, H.; Zhou, A.; Peng, F.; Yu, H.; Yang, J. *J. Colloid Interface Sci.* **2007**, *316*, 277.
(23) Chen, C.; Wang, X. *Ind. Eng. Chem. Res.* **2006**, *45*, 9144.
(24) Ruparelia, J. P.; Duttagupta, S. P.; Chatterjee, A. K.; Mukherjia, S. *Desalination* **2008**, *232*, 145.
(25) Di, Z. C.; Ding, J.; Peng, X. J.; Li, Y. H.; Luan, Z. K.; Liang, J. *Chemosphere* **2006**, *62*, 861.

as well as a wide range of organic solutes.[26−29] As a result, these materials have potential environmental importance as both fixed-phase (immobilized)[30,31] and dispersed-phase (mobile) sorbents. In the latter capacity, CNTs may facilitate the transport of co-contaminants.[26]

Several investigators have shown that treatment with strong oxidizing agents (e.g., HNO_3, HF/HNO_3, HNO_3/H_2SO_4, $KMnO_4$, H_2O_2, or NaClO) enhances the sorption properties of MWCNTs and SWCNTs toward heavy metals.[18−23] Because they create charged and hydrophilic surface functional groups, such oxidizing treatments also increase the colloidal stability and mobility of the individual CNTs.[32,33] To the extent that a mobile CNT may also carry sorbates to ecological or biological receptors, the CNT can act effectively as a "Trojan Horse", potentially transporting harmful contaminants into places that they would not otherwise reach. Thus, in the contexts of both engineered water treatment and proactive assessment of environmental risk, it is important to better understand the effect of oxidizing treatments on CNT sorption properties.

When CNTs are oxidized with oxidizing acids or other oxidants, a variety of oxygen-containing functional groups, such as carboxyl (−COOH), hydroxyl (C−OH), and carbonyl (C═O) groups can be grafted into its exposed surfaces,[32−35] preferentially at open ends and defect sites.[36] Work in our laboratories has shown that the extent of oxygen incorporation depends strongly upon the nature and strength of the oxidant as well as upon the duration and temperature of the oxidizing process.[26]

Several previous investigations have explored metal sorption by oxidized CNTs. For example, Lu and Chiu[21] studied the adsorption of Zn[II] from aqueous solution by SWCNTs and MWCNTs purified with NaClO at various temperatures. These authors showed that NaClO-treated CNTs had a greater specific sorption capacity for Zn[II] than powdered activated carbon. Li et al.[18] studied Cd[II] adsorption onto MWCNTs oxidized with H_2O_2, HNO_3, and $KMnO_4$ and showed that, at similar aqueous concentration, these oxidized MWCNTs (O-MWCNTs) sorbed between 2 and 10 times more Cd[II] than did the pristine, unoxidized MWCNTs (P-MWCNTs). Chen and Wang[23] reported that Ni[II] adsorption was much stronger with HNO_3−O-MWCNTs than with P-MWCNTs. Results from these studies clearly support the idea that oxidation enhances the sorption properties of MWCNTs toward metal cations, although the detailed relationship between changes in surface chemistry and sorption properties has not been elucidated.

In the research reported here, we studied the effects of surface oxidation on divalent metal cation adsorption from water, using Zn[II] and Cd[II] as probe sorbates and MWCNTs, natural char, and granular activated carbon (GAC) as sorbents. The decision to study Zn[II] and Cd[II] was motivated by the fact that these metals have simple speciation in contrast to other divalent cations such as Pb[II] and Hg[II]. In particular, at environmentally relevant pH values, both Zn[II] and Cd[II] exist principally as a divalent cation without covalent bonding to other elements. Although zinc can be present in aquatic environment in the form of Zn^{2+} $Zn(OH)^+$, $Zn(OH)_2(s)$, $Zn(OH)_3^-$, $Zn(OH)_4^{2-}$, and Zn_2OH^{3+},[2] the predominant species is Zn^{2+} (100% at pH 7 as calculated using Visual MINTEQ version 2.40b and using NIST Critically Selected Stability Constants of Metal Complexes Database version 8.0). Although details are not discussed here, cadmium species follow similar trends,[2] with 100% occurring as Cd^{2+} at pH 7 (as calculated using Visual MINTEQ version 2.40b and using NIST Critically Selected Stability Constants of Metal Complexes Database version 8.0).

In terms of solid-phase characterization, independent quantification of different surface oxide functional groups was obtained through surface analysis techniques based on X-ray photoelectron spectroscopy (XPS) used in conjunction with chemical derivatization techniques that target specific oxygen-containing functional groups on carbon surfaces.[37,38] We focused this research on MWCNTs rather than SWCNTs for three principal reasons: (1) MWCNTs are currently produced in greater quantities[39] and are therefore likely to be present in the environment in higher concentrations; (2) MWCNTs are much less expensive to produce and are therefore more likely to find continuing future use as commercial sorbents; and (3) for the MWCNTs studied, we have prior results which confirm that their length distribution and surface area were largely unaffected by treatment with nitric acid, permanganate, and hydrogen peroxide,[26] thus largely removing these physical properties as variables among our samples. In the present study, oxidation of CNT sorbents was accomplished primarily using HNO_3, due to its widespread use in functionalizing and purifying CNTs.[40,41] For comparison, we also studied sorption with MWCNTs that were prepared by other methods, such as with H_2SO_4/HNO_3 and $KMnO_4$. Studies were also conducted on MWCNT samples that were heated under argon to deliberately reduce their overall oxygen content and further modify the distribution of oxygen-containing functional groups.

2. Experimental Section

Sorbents. Granular activated carbon (GAC), natural char, and a suite of MWCNTs with varying surface oxygen content were selected as sorbents in this study. The GAC was a commercial material and used as received (F400, Calgon Carbon Corporation). Natural char (NC1) was prepared in our laboratory from a naturally charred pine log, as described by Nguyen et al.[42] NC1 and F400 samples were pulverized, homogenized, and sieved to pass 400 mesh (38 μm) or 200 mesh (75 μm) sieve screens, respectively. Untreated MWCNTs (diameter, 15 ± 5 nm; length, 5−20 μm; purity, 95%) were obtained from Nanolabs Inc., as were two commercial acid-treated samples described subsequently. Hereafter, we use the term "oxidized MWCNTs" (O-MWCNTs) to describe as-received untreated MWCNTs that have been exposed to oxidizing conditions, and we use the suffix designation "_F" to identify samples that have been subjected to furnace treatment under argon (as further described below).

(26) Cho, H.-H.; Smith, B. A.; Wnuk, J.; Fairbrother, H.; Ball, W. P. *Environ. Sci. Technol.* **2008**, *42*, 2899.
(27) Peng, X. L.; Yanhui; Luan, Z.; Di, Z.; Wang, H.; Tian, B.; Jia, Z. *Chem. Phys. Lett.* **2003**, *376*, 154.
(28) Yang, K.; Zhu, L. Z.; Xing, B. *Environ. Sci. Technol.* **2006**, *40*, 1855.
(29) Zhang, S.; Shao, T.; Bekaroglu, S. K.; Karanfil, T. *Environ. Sci. Technol.* **2009**, *43*, 5719.
(30) Majumder, M.; Chopra, N.; Hinds, B. *J. Am. Chem. Soc.* **2005**, *127*, 9062.
(31) Majumder, M.; Zhan, X.; Andrews, R.; Hinds, B. J. *Langmuir* **2007**, *23*, 8624.
(32) Smith, B.; Wepasnick, K.; Schrote, K. E.; Bertele, A. R.; Ball, W. P.; O'Melia, C.; Fairbrother, D. H. *Environ. Sci. Technol.* **2009**, *43*, 819.
(33) Smith, B.; Wepasnick, K.; Ball, W. P.; Fairbrother, D. H. *Langmuir* **2009**, *25*, 9767.
(34) Peng, Y.; Liu, H. *Ind. Eng. Chem. Res.* **2006**, *45*, 6483.
(35) Rosca, I. D.; Watari, F.; Uo, M.; Akasaka, T. *Carbon* **2005**, *43*, 3124.
(36) Li, X.; Niu, J.; Zhang, J.; Li, H.; Liu, Z. *J. Phys. Chem. B* **2003**, *107*, 2453.
(37) Langley, L. A.; Villanueva, D. E.; Fairbrother, D. H. *Chem. Mater.* **2006**, *18*, 169.
(38) Langley, L. A.; Fairbrother, D. H. *Carbon* **2007**, *45*, 47.
(39) CientificaNanotubes,http://www.cientifica.com/www/summarys/Nanotubes_2004_Ex Sum.pdf, **2004**.
(40) Zhang, X.; Sreekumar, T. V.; Liu, T.; Kumar, S. *J. Phys. Chem. B* **2004**, *108*, 16435.
(41) Li, Y.; Zhang, X.; Luo, J.; Huang, W.; Cheng, J.; Luo, Z.; Li, T.; Lui, F.; Xu, G.; Ke, X.; Li, L.; Geise, H. J. *Nanotechnology* **2004**, *15*, 1645.
(42) Nguyen, T. H.; Cho, H.-H.; Poster, D. L.; Ball, W. P. *Environ. Sci. Technol.* **2007**, *41*, 1212.

For ease of reference, we refer to the as-received untreated MWCNTs as "pristine MWCNTs" (P-MWCNTs).

In this study, we used O-MWCNTs that had been prepared with potassium permanganate ($KMnO_4$), sulfuric acid/nitric acid (H_2SO_4/HNO_3), and nitric acid (HNO_3) at a range of concentrations. In addition, we purchased two pretreated materials from the commercial supplier (Nanolabs, Inc.): H_2SO_4/HNO_3-treated O-MWCNTs and O-MWCNTs that were treated with H_2SO_4/HNO_3 in a microwave oven. The various oxidation methods used are further described below.

H_2SO_4/HNO_3. A total of 400 mg of MWCNTs was added to 32 mL of a 3:1 (v:v) mixture of concentrated H_2SO_4 and HNO_3. The mixture of MWCNTs and acid was then heated at 70 °C for 8 h without stirring. O-MWCNTs from Nanolabs, Inc. were prepared using either H_2SO_4/HNO_3 as described above or through a proprietary combination of microwave heating and H_2SO_4/HNO_3 treatment. These samples are subsequently referred to as NL-H_2SO_4/HNO_3 and NL-$\mu\lambda/H_2SO_4/HNO_3$, respectively.

$KMnO_4$. Following a procedure outlined in Hiura et al.,[43] MWCNTs (100 mg) were added to a 0.5 M H_2SO_4 solution (200 mL), and the solution was heated to 150 °C. To the heated solution, a 0.8 M $KMnO_4$/0.5 M H_2SO_4 solution (200 mL) was added dropwise. The final mixture was then refluxed for 5 h while stirring. After cooling to room temperature, 10 mL of concentrated HCl was added to complex the MnO_2 byproduct.

HNO_3. MWCNTs prepared with HNO_3 were refluxed at 12 different HNO_3 concentrations, ranging from 10% to 70% w/w using methods previously described by Cho et al.[26] The 12 acid concentrations used are shown in the Supporting Information (Table S1).

Furnace Treatment. We further treated three O-MWCNTs that had initially high oxygen content by heating them to high temperature under an inert gas flow. These samples were placed in an Inconel-lined quartz-tube graphitizing furnace operated at 500 °C under a constant flow of 100% argon gas for a period of 12 h. The three samples thus treated were O-MWCNTs that had been prepared with 70% w/w HNO_3, $KMnO_4$, and the commercial $\mu\lambda/H_2SO_4/HNO_3$ process. These three furnace-treated O-MWCNTs are hereafter referred to as 70%-HNO_3-b_F, $KMnO_4$_F, and NL-$\mu\lambda/H_2SO_4/HNO_3$_F.

O-MWCNT Purification. Commercial MWCNTs were used as received (without further modification). O-MWCNTs prepared in our laboratories were further purified with a procedure that we had previously developed and reported[32] for removal of residual acids, metallic byproducts, and amorphous carbon. Briefly, all O-MWCNTs were cleaned extensively by repeatedly centrifuging (Powerspin LX, Unico) and decanting until the resistivity of the supernatant was greater than 0.5 MΩ and the pH stabilized at a value between 6 and 7. The O-MWCNTs were then air-dried overnight in an oven at 100 °C. Once dry, the O-MWCNTs were pulverized in a ball-mill (MM200, Retsch) for 15 min.

Characterization of Pristine and Oxidized MWCNTs. The MWCNTs' chemical composition was determined using XPS (PHI 5400 system).[32,33] For XPS, MWCNTs were adhered to double-sided copper tape and mounted onto a sample stub. Care was taken to ensure that the MWCNTs completely covered the copper tape. In all XPS experiments, Mg Kα (1253.6 eV) X-ray radiation was generated from a Φ 04-500 X-ray source. Ejected photoelectrons were analyzed using a hemispherical electron energy analyzer operating at a pass energy of 178.95 and 0.250 eV/step. The distribution of oxygen-containing functional groups present on the O-MWCNT surface was quantified using vapor-phase chemical derivatization in conjunction with XPS. In brief, trifluoracetic anhydride, trifluoroethyl hydrazine, and trifluoroethanol were used to assay the concentration of surface-bound hydroxyl, carbonyl, or carboxylate groups, respectively, using methods previously developed and applied in our laboratory.[32,33,37,38]

For Brunauer−Emmett−Teller (BET) measurements of specific surface area (SSA), N_2 adsorption data at 77 K were obtained using a high-resolution gas adsorption analyzer with high-vacuum capacity (5.0×10^{-7} Pa) (ASAP 2010, Micromeritics).[44] Following previously established protocols for black carbon,[42] all samples were outgassed at 300 °C for 5 h prior to analysis.

Sorption Experiments. Analytical-grade zinc nitrate or cadmium nitrate (Sigma-Aldrich) was used to prepare a 10 mM stock solution from which subsequent dilutions were made for purposes of spiking sorption vessels. Weighed amounts (5 mg) of MWCNTs were introduced into 5 mL polypropylene tubes (Spectrum Chemical) to which 2 mL of high concentration zinc/cadmium spiking solution (3 mM $Zn(NO_3)_2$/1.8 mM $Cd(NO_3)_2$) were added, creating initial concentrations (C_0) ranging from 0.08 to 3 mM for Zn[II] and from 0.05 to 1.8 mM for Cd[II]. The ionic strength (I) was fixed at 0.01 M for all experiments, using $NaNO_3$ as background electrolyte. The initial pH was between 6.5 and 6.8 for all solutions, except those used in special pH studies described in the Supporting Information. For most of our isotherm results (including all those reported in the main text), no pH buffer was used. Independent experiments on selected samples of both pristine and oxidized (NL-$\mu\lambda/H_2SO_4/HNO_3$) samples with larger liquid volumes revealed that, at the given dose (1 mg CNT/mL), final pH values consistently fell in the range of 5.9−6.1. Additionally, the independent studies of pH effect (Figure S7 in the Supporting Information) for a uniform $[Zn^{2+}]_0$ of 2.9 confirmed that pH changes in the range of 5.0−6.8 had no significant effect on Zn^{2+} sorption.

The resulting solutions were mixed by end-over-end rotation in a dark, temperature controlled (23 ± 0.5 °C) environmental chamber, with 2 days of equilibration used for all sorption studies reported. We confirmed that equilibrium conditions were reasonably well achieved during the 2 day experiments through kinetic experiments conducted with MWCNTs, GAC, and NCA at $[Zn^{2+}]_0 = 0.09$ mM. These results, shown in Figure S3 in the Supporting Information, confirmed that adsorption was effectively complete after just 2 hours, with adsorbed concentrations remaining approximately constant over the full range of times tested (2 h to 5 days) for all three materials. For example, ratios of sorbed to aqueous concentration (distribution coefficients, or K_d values) for P-MWCNTs were 23.3 ± 0.4 mL/g and 23.8 ± 0.9 mL/g at 2 and 5 days, respectively ($K_d = q_e/C_e$, where q_e [mg/g] and C_e [mg/L] are the sorbed- and aqueous-phase equilibrated concentrations). These measured K_d values are statistically equivalent at a significance level, α, of 5% (two-sided t test).

After equilibration, the MWCNTs were separated from the liquid phase by passing the mixture through a 0.2 μm Nylon filter (Corning Co.). Control experiments using Zn[II] in solution without MWCNTs showed that the Nylon filters sorbed less than 0.2% of the Zn[II]. Other control experiments using colloidal suspensions of O-MWCNTs in the absence of Zn[II] showed that the Nylon filters removed 99.99% of the O-MWCNTs from solution. In these experiments, the concentration of MWCNTs in suspension was quantified by measuring the UV absorption at 500 nm.[33] Following solid/liquid separation, the aqueous concentration of Zn[II] was determined using a flame atomic absorption spectrometer (model 100, Perkin-Elmer). The mass of sorbed Zn[II] was determined by subtracting the mass of Zn[II] in solution from the initial aqueous Zn[II] mass. Mass losses to labware as determined through "blank" experiments carried out in the absence of MWCNTs revealed < 1.0% loss of Zn[II] mass in all cases when polypropylene centrifuge tubes were used. (By contrast, preliminary testing with 5 mL glass tubes revealed 50% loss of Zn[II] mass at 0.09 mM $[Zn[II]]_0$, clearly indicating that Zn[II] adsorbed to the glass walls of the vessel and causing us to abandon this protocol.) To test the importance of the MWCNT

(43) Hiura, H.; Ebbesen, T. W.; Tanigaki, K. *Adv. Mater.* **1995**, *7*, 275.

(44) Micromeritics, Application #104, Determining free-space values for ASAP series micropore analyses.

aggregation state on equilibrium, some samples were sonicated prior to the addition of Zn[II]; see the Supporting Information. Results from these studies (Figure S4 in the Supporting Information) suggest that the aggregation state has little or no effect on MWCNT sorption properties with metal cations. These results are in agreement with our prior work on naphthalene sorption by MWCNTs,[26] and suggest minimal effect from any reduction of available surface area. This is in contrast to postulations by Zhang et al. in the context of organic chemical sorption by CNTs,[29] but it is actually consistent with their evidence for substantial mesopore and macropore volume within MWCNT aggregates, which could help to keep most surface sites accessible to long-term (equilibrium) sorption, even after aggregation. Thus, and although one should expect impacts of aggregation on the rate of approach to equilibrium (owing to increases of the diffusion length scale), equilibrium was apparently not affected. Moreover, our kinetic studies (Figure S3 in the Supporting Information) suggest that rate limitations were also not especially severe in the systems studied here.

To analyze the influence of pH on adsorption, selected samples were brought to initial pH values ranging from 2.0 to 6.9 by adding appropriate amounts of 1 M HCl and 1 M NaOH prior to the addition of O-MWCNTs. These samples were then studied with respect to their sorption behavior at high aqueous concentrations of Zn[II] ($[Zn[II]]_0 = 2.9$ mM).

Modeling Adsorption Isotherms. To model divalent metal cation adsorption onto surfaces, we adopted the widely accepted Langmuir isotherm model, both in its simplest (one-site) form, which is convenient for qualitative comparison of isotherms, and in the following more complex (multisite) form, which is better for exploring mechanistic aspects of Zn[II] sorption with selected sorbents:

$$q_e = \sum_{i=1}^{n} q_{e,i} = \sum_{i=1}^{n} \frac{q_{max,i} K_{L,i} C_e}{1 + K_{L,i} C_e} \quad (1)$$

where n is the assumed number of distinct surface "site types" that are active in sorption (e.g., carboxylate groups). In eq 1, C_e is the aqueous phase concentration of sorbate at equilibrium ($mmol_{sorbate}/L$), q_e is the total adsorbed concentration of sorbate ($mmol_{sorbate}/g_{sorbent}$), and $q_{e,i}$ is the concentration of adsorbate associated with site type "i" but reported on the basis of *total* sorbent mass ($mmol_{sorbate}/g_{sorbent}$). $q_{max,i}$ is the maximum sorption capacity (mmol/g), and $K_{L,i}$ is the adsorption affinity of each surface "site type", as measured by the Langmuir sorption constant (L/mg).

The assumptions behind eq 1 are well-known:[45,46] (1) the adsorption energy for a given site type is constant and independent of surface coverage; (2) adsorption occurs only on localized surfaces sites, with no interaction between adsorbate molecules; and (3) adsorption is limited to the formation of a monolayer of adsorbed species on the surface. For most real sorbents such as O-MWCNTs, the types of surface sites can be numerous and varied if one recognizes that divalent cations such as Zn^{2+} are likely to coordinate with more than one surface species at a time and that the relative locations of the various surface species will therefore affect sorption energetics. In this regard, we do not know the locations of the various functional groups and must therefore "lump" all sites with a given functionality into a single "site type". Such lumping will not affect our interpretations so long as the spatial proximities of the different functional groups either (1) do not vary substantially with regard to their statistical distribution among the various materials studied or (2) do not have substantial effect on sorption energetics.

(45) Weber, W. J., Jr.; DiGiano, F. A. *Process Dynamics in Environmental Systems*; John Wiley & Sons, Inc.: New York, 1996.
(46) Adamson, A. W.; Gast A. P. *Physical Chemistry of Surfaces*, 6th ed.; John Wiley & Son, Inc.: New York, 1997.

3. Results and Discussion

Effect of Surface Oxidation on Physicochemical Properties of MWCNTs. The overall extent of oxidation that occurs at the MWCNT surface was observed to increase systematically with the concentration of HNO_3 (10 to 70% w/w) used to oxidize P-MWCNTs. (See Tables 1 and 2 and Table S1 in the Supporting Information. Combined data for all materials are in Table S1.) For example, O-MWCNTs treated with HNO_3 (70%) exhibited 10.3% surface oxygen (based on XPS measurements of atom %), whereas the surface oxygen concentration for the P-MWCNTs was only 2.1% (Table 1). Between these limits, surface oxygen contents generally increased monotonically, as reported in our prior work.[26,32,33] The precision with which the various treatment protocols reproduced oxygen content was in the range of 15−40%, as suggested by surface oxygen concentrations that varied between 7.0% and 10.3% for triplicate samples treated with 70% HNO_3 and between 6.9% and 8.1% for triplicate samples treated with 50% or 53% HNO_3 (see Table S1 in the Supporting Information). O-MWCNTs prepared by the other methods (H_2SO_4/HNO_3, $KMnO_4$, NL-H_2SO_4/HNO_3, NL-$\mu\lambda$/H_2SO_4/HNO_3) exhibited surface oxygen contents between 4.7% and 10.3% (Table S1 in the Supporting Information). For selected O-MWCNTs, furnace treatment at 500 °C under argon caused the loss of between 32% and 58% of the surface oxygen present. (See samples identified as "_F" in Table S1 in the Supporting Information.) XPS analysis after chemical derivitization (Table 2) showed that the vast majority of loss from these "_F" samples was from sites characterized as either "COOH" or "unaccounted residual oxygen", with the latter corresponding to oxygen-containing functional groups other than hydroxyl, carbonyl, and carboxyl whose concentrations cannot be assayed using our methods. It should be noted that this analysis will not distinguish contributions from any amorphous carbon that may be present at the CNT surface.

In a previous paper,[26] we presented atomic force microscope (AFM) and transmission electron microscope (TEM) results which demonstrated that oxidation with HNO_3 does not shorten the O-MWCNTs to a significant extent compared to the P-MWCNTs and that the O-MWCNTs remain structurally intact after oxidation. In addition, the BET-measured surface area (BET-SA) of pristine and O-MWCNTs were also found to be statistically the same (270 m^2/g vs 269 ± 15 m^2/g) after HNO_3 and $KMnO_4$ treatment, although statistically significant decreases in SA (195 m^2/g and 210 m^2/g) were observed after treatment with H_2SO_4/HNO_3 and NL- H_2SO_4/HNO_3, respectively. (See Table S1 in the Supporting Information for details.) Overall, the physical similarity of pristine and O-MWCNTs suggests that changes in equilibrium sorption capacity upon oxidation were principally caused by changes in surface chemistry. To further characterize the O-MWCNT surface chemistry, several samples were sent to an outside laboratory (Geology Department, Virginia Polytechnic Institute and State University, Blacksburg, VA) for analysis by Raman spectroscopy performed at $\lambda = 514.57$ nm. It should be noted that although Raman is a valuable tool for characterizing SWCNTs, it less useful for MWCNTs because the radial breathing modes are too weak to be observed. Nonetheless, the data provided some insights on our samples. In particular, the Raman spectra of four MWCNTs (Figure S5 in the Supporting Information) showed two characteristic peaks at around 1333 cm^{-1} (D band) and 1585 cm^{-1} (G band). The G band generally originates from in-plane tangential stretching of the carbon−carbon bonds in graphenic sheets, while the D band is due to either defect sites in the hexagonal framework of

Table 1. Parameters for Langmuir Isotherm Equation Based on Fits to Zn[II] and Cd[II] Sorption Data for Carbonaceous Materials, Including MWCNTs That Had Been Oxidized to Varying Extents

	sorbent									
sorbate		treatment[a]	surface oxygen (%) by XPS	N^b	q_{max} (mmol/g)[c]	q_{max}/BET-SA (μmol/m^2)[c,d]	K_L (L/mmol)[c]	$q_{max}K_L$ (L/g)[c]	MWSE[e]	r^2
Zn[II]	natural char (NC1)		23.0	21	0.31 ± 0.011	6.74 ± 0.24	1.27 ± 0.16	0.40 ± 0.033	0.015	0.98
	activated carbon (F400)		8.0	21	0.51 ± 0.022	0.51 ± 0.022	2.21 ± 0.26	1.11 ± 0.094	0.007	0.98
	pristine MWCNT		2.1	21	0.14 ± 0.013	0.52 ± 0.048	1.11 ± 0.16	0.15 ± 0.022	0.013	0.97
	O-MWCNT	18%-HNO_3	4.7	14	0.16 ± 0.011	0.59 ± 0.041	1.59 ± 0.23	0.25 ± 0.033	0.007	0.98
		25%-HNO_3	5.1	14	0.18 ± 0.022	0.67 ± 0.082	2.74 ± 0.41	0.50 ± 0.061	0.008	0.98
		42%-HNO_3	7.0	14	0.23 ± 0.013	0.86 ± 0.048	1.81 ± 0.27	0.42 ± 0.053	0.010	0.99
		53%-HNO_3-a	8.0	14	0.24 ± 0.021	0.89 ± 0.078	3.32 ± 0.32	0.80 ± 0.044	0.002	0.99
		70%-HNO_3-a	10.3	14	0.27 ± 0.012	1.00 ± 0.045	3.92 ± 0.49	1.05 ± 0.10	0.004	0.98
		H_2SO_4/HNO_3	10.2	14	0.24 ± 0.034	1.23 ± 0.17	3.67 ± 0.35	0.88 ± 0.073	0.015	0.99
		NL-H_2SO_4/HNO_3	6.1	14	0.21 ± 0.020	1.00 ± 0.095	2.76 ± 0.26	0.59 ± 0.042	0.015	0.99
		NL-$\mu\lambda$/ H_2SO_4/HNO_3	10.8	14	0.23 ± 0.010	0.90 ± 0.039	2.05 ± 0.33	0.48 ± 0.063	0.013	0.97
Cd[II]	natural char (NC1)		23.0	21	0.16 ± 0.014	3.48 ± 0.30	2.24 ± 0.26	0.35 ± 0.034	0.009	0.98
	activated carbon (F400)		8.0	21	0.23 ± 0.022	0.23 ± 0.022	5.21 ± 0.50	1.21 ± 0.081	0.012	0.97
	pristine MWCNT		2.1	21	0.05 ± 0.012	0.19 ± 0.044	2.80 ± 0.31	0.13 ± 0.012	0.008	0.99
	O-MWCNT	53%-HNO_3-b	8.3	14	0.18 ± 0.012	0.67 ± 0.045	10.1 ± 0.91	1.77 ± 0.13	0.008	0.99
		H_2SO_4/HNO_3	10.2	14	0.22 ± 0.024	1.13 ± 0.012	12.9 ± 2.47	2.79 ± 0.47	0.014	0.96
		NL-$\mu\lambda$/ H_2SO_4/HNO_3	10.8	14	0.21 ± 0.011	0.82 ± 0.043	16.7 ± 1.97	3.53 ± 0.37	0.009	0.98

[a] Treatments were as described in text. "-a" and "-b" designation on some samples signifies the first and second, respectively, of replicate production batches. See Table S1 in the Supporting Information for a complete list of samples, including listings of % oxygen by XPS, BET-SA, and Zn[II] K_d data (at C_e = 2.8 mM) where available. [b] N = number of observations. [c] Shown are values ± 2 standard deviations. [d] Calculation uses BET-SA values shown in Table S1 in the Supporting Information. [e] MWSE = mean weighted square error = $1/\nu\sum[(q_{measured} - q_{model})^2]/q_{measured}^2$, where ν is the number of degrees of freedom; here $\nu = N - 2$.

Table 2. K_d Data at $C_e \cong 2.8$ mM and Surface Functional Group Distribution for MWCNTs That Had Been Oxidized to Varying Extents[a]

treatment[b]		K_d (mL/g)[c]	% $O_{T,obsd}$[d]	% $O_{COOH,obsd}$[d]	% $O_{C-OH,obsd}$[d]	% $O_{C=O,obsd}$[d]	% $O_{residual,obsd}$[d]
pristine	+	36.9 ± 1.9	2.1	0.9	0.6	0.8	−0.2
10%-HNO_3	○	57.6 ± 5.1	3.0	1.5	0.6	0.8	0.1
20%-HNO_3	○	63.3 ± 0.2	4.3	1.9	0.8	0.9	0.6
30%-HNO_3	○	59.9 ± 5.4	5.3	2.4	0.5	0.8	1.5
40%-HNO_3	○	56.5 ± 4.6	5.5	2.7	0.6	1.0	1.3
50%-HNO_3	○	75.8 ± 2.5	8.1	4.3	1.1	1.4	1.3
60%-HNO_3	○	73.1 ± 0.5	7.6	4.2	1.0	1.2	1.2
70%-HNO_3-a	○	70.2 ± 3.3	9.5	3.4	0.9	1.1	4.1
70%-HNO_3-b	○	62.5 ± 4.1	7.0	2.7	0.7	1.1	2.5
70%-HNO_3-b_F[e]	●	46.3 ± 2.3	4.3	1.3	0.6	1.2	1.2
H_2SO_4/HNO_3	♦	87.3 ± 2.7	10.2	5.8	1.0	1.6	1.8
NL-H_2SO_4/HNO_3	■	74.1 ± 1.1	6.1	3.6	0.8	1.6	0.1
NL-$\mu\lambda/H_2SO_4/HNO_3$	▼	75.4 ± 2.6	10.8	5.3	1.3	2.6	1.6
NL-$\mu\lambda/H_2SO_4/HNO_3$_F[e]	▲	45.8 ± 2.6	4.7	1.3	1.4	1.8	0.2
$KMnO_4$	★	81.8 ± 0.2	8.4	5.5	0.8	2.1	0
$KMnO_4$_F[e]	⬢	32.9 ± 2.2	5.7	0.5	0.8	2.1	2.3

[a] Note: For reasons described in the text, samples overlap with those of Table 1 only for the following four samples: pristine, H_2SO_4/HNO_3, NL-H_2SO_4/HNO_3, and NL-$\mu\lambda/H_2SO_4/HNO_3$. See Table S1 in the Supporting Information for complete list of materials. [b] Treatments were as described in text. "-a" and "-b" designation on some samples signifies the first and second, respectively, of replicate production batches. See Table S1 in the Supporting Information for a complete list of samples, including listings of % oxygen by XPS, BET-SA, and Zn[II] K_d data (at C_e = 2.8 mM) where available. [c] Distribution coefficient (K_d) of Zn[II] on the MWCNTs at $[Zn[II]]_e \cong 2.8$ mM, I = 0.01 M, and pH = 6.5−6.8. Shown are the average values based on three replicates. [d] % $O_{T,obsd}$ is the total atom % surface oxygen by XPS as reported in Tables 1 and the Supporting Information. Remaining columns show functional group distribution as obtained through CD/XPS analysis. (See text.) % $O_{residual,obsd}$ is calculated by subtracting the sum of individual functional group percentages from % $O_{T,obsd}$. [e] Samples ending with "_F" were furnace-treated under argon at 400 °C.

MWCNTs or the presence of amorphous carbon.[47] For NL-H_2SO_4/HNO_3, the Raman analysis indicated an I_D/I_G band ratio that was higher than that observed with P-MWCNTs (I_D/I_G = 0.94 vs 0.62). Although we did not obtain Raman spectra for O-MWCNTs treated with HNO_3, Curran et al. reported that MWCNT samples exposed to HNO_3 also showed an increase in I_D/I_G band ratio.[48] In general, such an increase in I_D/I_G with oxidation suggests an increase in structural disorder due to the sidewall damage that accompanies oxidation. Interestingly, however, the NL-$\mu\lambda/H_2SO_4/HNO_3$ sample did not follow this same trend, but rather had a lower I_D/I_G band ratio (I_D/I_G = 0.51 vs 0.62). Also, in contrast to the other H_2SO_4/HNO_3 samples, the BET-SA of NL-$\mu\lambda/H_2SO_4/HNO_3$ was not substantially reduced relative to the untreated starting material.

Comparison of Zn[II] and Cd[II] Sorption Isotherms among GAC, NC1, P-MWCNTs, and O-MWCNTs. To simplify a qualitative comparison of results, we used the simple one-site Langmuir adsorption isotherm equation (n = 1 in eq 1) to model Zn[II] and Cd[II] adsorption by pristine, O-MWCNTs, and the other carbonaceous materials (NC1, GAC). Results are shown in Figure 1, with fitted parameters and statistics as given in Table 1. On a per mass of carbon basis (i.e., without yet accounting for the effects of surface area), the maximum adsorption capacities (q_{max}) for both Zn[II] and Cd[II] increased in the

(47) Ying, Y. M.; Saini, R. K.; Liang, F.; Sadana, A. K.; Billups, W. E. *Org. Lett.* **2003**, *5*, 1471.
(48) Curran, S. A.; Talla, J. A.; Zhang, D.; Carroll, D. A. *J. Mater. Res.* **2005**, *20*, 3368.

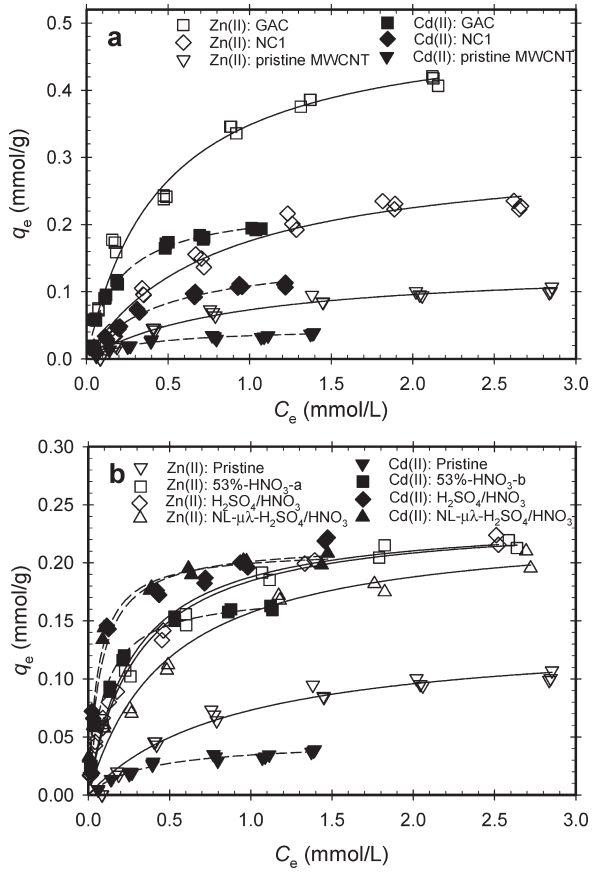

Figure 1. Zn[II] and Cd[II] sorption isotherms for carbonaceous materials: (a) pristine MWCNT, natural char (NC1), and granular activated carbon (F400) and (b) pristine MWCNT and three different treated O-MWCNTs (53%-HNO_3-a, -b, H_2SO_4/HNO_3, and NL-$\mu\lambda/H_2SO_4/HNO_3$). Lines (solid, Zn[II]; dotted, Cd[II]) through the data are based on fits obtained using the Langmuir adsorption model ($n = 1$, eq 1). Isotherm model parameters and relevant statistics for the Langmuir model fits are reported in Table 1. The surface oxygen concentrations determined by XPS for the various samples are given in Table 1.

following order: pristine MWCNT < NC1 < GAC (F400) (Figure 1a). And q_{max} values for P-MWCNTs were substantially less than those of the O-MWCNTs. Note that Cd[II] sorption capacity with O-MWCNTs was similar to that of Zn[II], despite the fact that Cd[II] sorption capacity was 2.8 times less than that of Zn[II] on the P-MWCNTs (Figure 1b). Apparently, surface oxidation affected the sorption of Cd[II] more strongly than it affected the sorption of Zn[II].

It is also useful to consider the effect of surface area by comparing q_{max} values after surface area normalization. For this purpose, we applied the BET-SA results presented in Table S1 in the Supporting Information. This analysis revealed that q_{max} values of Zn[II] for P-MWCNTs and GAC (F400) were essentially equivalent on a BET-SA-normalized basis, despite their approximately 3.6-fold difference on a per mass basis. Overall, the BET-SA-normalized capacity (q_{max}/BET-SA) followed the order GAC (0.51 μmol/m^2) $\cong$ pristine MWCNT (0.52 μmol/m^2) $\ll$ NC1 (6.74 μmol/m^2) for Zn[II], and pristine MWCNT (0.19 μmol/m^2) < GAC (0.23 μmol/m^2) $\ll$ NC1 (3.48 μmol/m^2) for Cd[II] (Table 1). The high q_{max}/BET-SA values for NC1 (Figure S6 in the Supporting Information) reflect the influence of surface chemistry; at 23% oxygen content, this material was by far the most oxidized sorbent. Although prior XPS studies with NC1 have revealed the presence of carboxylate groups,[38] the XPS data from these sites cannot be interpreted as simply as can the data from CNTs owing to the greater chemical and physical complexity of the NC1 material. Nonetheless, the GAC and NC1 data do confirm that the extent of surface oxidation and the surface area are both important factors that affect the sorption of divalent metals by CNTs and other carbonaceous sorbents.

Surface-area normalization also provided a useful means of considering the sorption results obtained with acid-treated O-MWCNTs. Zn[II] and Cd[II] q_{max} values for these oxidized materials were higher than those of the P-MWCNTs but still less than or similar to those observed with F400 and NC1 (Figure 1b and Table 1) when compared on a mass basis. On the other hand, the BET-SA-normalized data (shown in Table S1 and Figure S6 in the Supporting Information) indicated that CNT sorption was actually stronger per unit area. For example, considering the O-MWCNT treated with H_2SO_4/HNO_3, which is one of the most highly oxidized O-MWCNTs for which we have both Zn[II] and Cd[II] data, we note that q_{max}/BET-SA values for Zn[II] and Cd[II] were 2.5 times higher and 5 times higher, respectively, than the values observed for GAC (1.23 μmol/m^2 vs 0.51 μmol/m^2 for Zn and 1.13 μmol/m^2 vs 0.23 μmol/m^2 for Cd). Lu and coworkers[20,21] showed similar results for Zn[II], finding that the BET-SA-normalized q_{max} observed with MWCNT "purified" by NaClO (1.68 μmol/m^2) was 6.7 times higher than that observed with a powdered activated carbon (0.25 μmol/m^2).

In terms of practical considerations of sorbents for water treatment, it is important to consider that the current cost of MWCNTs and GAC is roughly \$120/g and \$0.08/g, respectively. Thus, the practical use of MWCNTs over GAC is not warranted for any practice that does not effectively reuse the sorbent. In this regard, Lu et al. have reported that the reversibility of Zn[II] sorption onto CNTs is much better (i.e., the ion exchange much faster), as should be expected owing to the vastly reduced diffusion length scales. These findings indicate that CNTs can be more easily reused through many cycles of water treatment and regeneration.[49] It is thus conceivable that CNTs may find specialized use for water treatment, especially if the cost of CNTs continues to decrease and if durable materials can be developed to facilitate CNT adsorption and regeneration over multiple cycles. The incorporation of CNTs into the surface of larger scale ion exchange media or into water treatment membranes represents two such possibilities.

Effect of MWCNT Oxidation on Zn[II] Sorption. The remainder of this paper focuses on elucidating the role that surface chemistry plays in determining the sorption properties of pristine and O-MWCNTs toward divalent metal cations, using Zn[II] as a prototypical example. Initially, we considered the influence of oxygen concentration, as determined by XPS, on the MWCNTs' sorption capacities. We then conducted a more quantitative analysis of the role that different functional groups at the MWCNT surface play in regulating sorption properties, including the development of a two-site Langmuir adsorption model to predict Zn[II] sorption capacity on the basis of detailed information about surface functional group densities.

To provide a more detailed understanding of the effect of MWCNT oxidation on Zn[II] sorption, we conducted full sorption isotherms with Zn[II] using nine MWCNT samples: P-MWCNTs, five O-MWCNTs treated with different concentrations of HNO_3 (ranging from 18% to 70%, and three O-MWCNTs treated with other oxidants (H_2SO_4/HNO_3, NL-H_2SO_4/HNO_3, and NL-$\mu\lambda/H_2SO_4/HNO_3$) (Table 1 and Figure 2). For the five O-MWCNTs treated with HNO_3, results

(49) Lu, C.; Chiu, H.; Bai, H. *J. Nanosci. Nanotechnol.* **2007**, *7*, 1647.

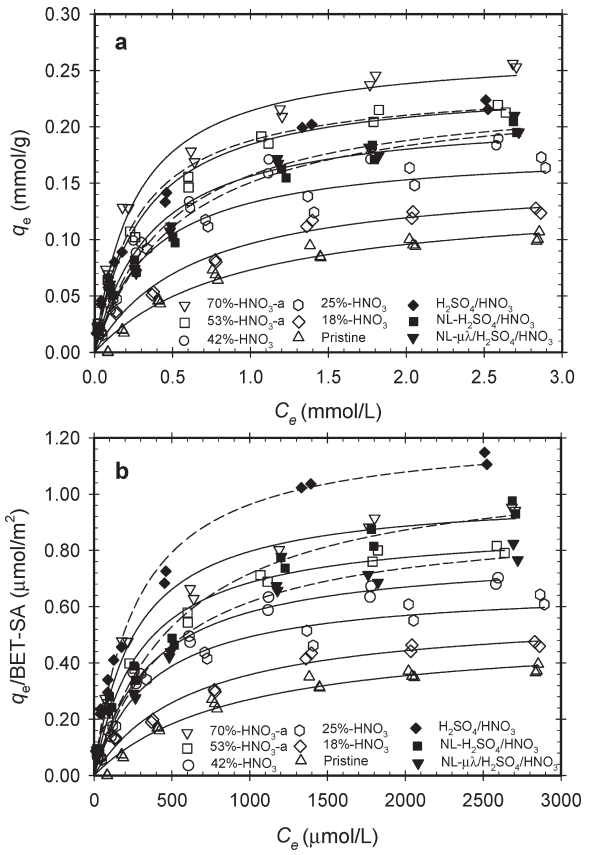

Figure 2. Sorption isotherms for Zn[II] with pristine and oxidized MWCNTs. Lines (solid, pristine and HNO_3; dotted, other oxidants) through the data are based on fits obtained using the Langmuir adsorption model ($n = 1$, eq 1). Isotherm model parameters and relevant statistics for the Langmuir model fits are reported in Table 1. The atom % surface oxygen concentration measured by XPS for the various samples is given in Table 1.

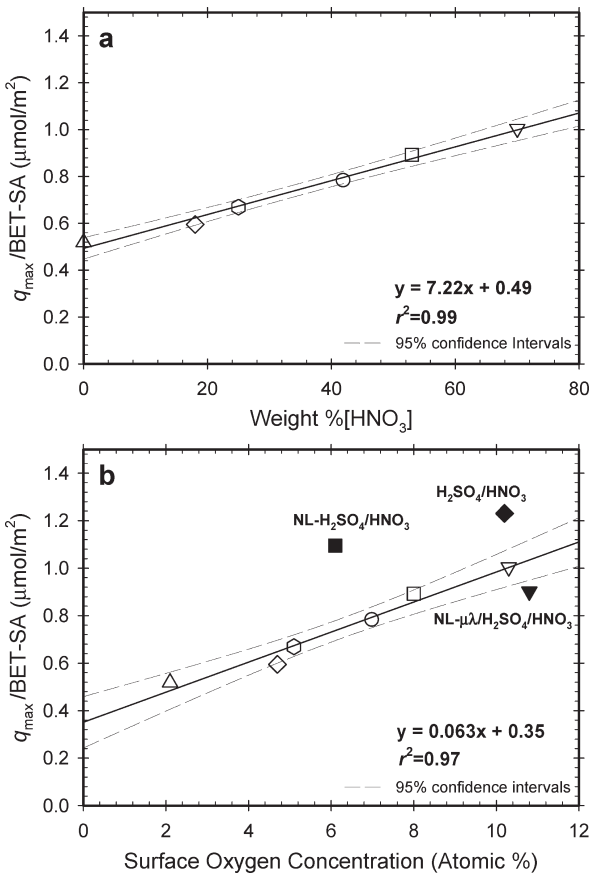

Figure 3. (a) Maximum adsorption capacity (q_{max}) for Zn[II] normalized by BET-SA (q_{max}/BET-SA) as determined by eq 1 plotted against the nitric acid concentration used to oxidize the MWCNTs. (b) q_{max}/BET-SA plotted against surface oxygen concentration for all oxidative methods used. In both figures, the open symbols represent MWCNTs oxidized with HNO_3 and the solid symbols represent MWCNTs oxidized with either H_2SO_4/HNO_3 or $\mu\lambda/H_2SO_4/HNO_3$.

clearly show a systematic increase in the extent of Zn[II] adsorption with increasing HNO_3 concentration. For the other three O-MWCNTs, Zn[II] sorption isotherms also increased relative to P-MWCNTs. Analysis of Table 1, however, indicates that, of the eight O-MWCNTs studied, the maximum adsorption capacity (q_{max}) of Zn[II] with the most highly oxidized O-MWCNT (10.3% oxygen) was only 2 times greater than that of the least oxidized O-MWCNT (2.1% oxygen), despite the fact that the surface oxygen concentration increased 5-fold (Table 2). As elaborated subsequently, this increase is smaller than would be expected based on a simple zero-intercept linear correlation and suggests that surface oxygen concentration and surface area are not the only factors controlling sorption.

In Figure 3, linear regressions are shown for q_{max}/BET-SA values with both (a) the strength of HNO_3 used during oxidation and (b) the total surface oxygen concentration measured for all of the different oxidative methods used. For the HNO_3-treated samples, the correlation between q_{max}/BET-SA and oxygen concentration was strong among all O-MWCNTs (see Figure 3a). Figure 3b reveals, however, that O-MWCNTs treated by other oxidative methods fell outside the simple regression. For example, the two O-MWCNTs treated with H_2SO_4/HNO_3 had significantly different sorption capacities than O-MWCNTs oxidized with 70% HNO_3, despite the fact that all three O-MWCNTs exhibited a comparable concentration of surface oxygen.

In both panels of Figure 3, the regression lines have a substantial positive y-intercept. The existence of such an intercept revealed that Zn[II] sorption did not occur exclusively on sites associated with surface oxygen functional groups, suggesting contributions from nonoxygenated surfaces. In addition, the outliers of Figure 3a indicated a need to also consider the relative roles played by different types of surface oxygen, as could be explored through independent quantification of the different kinds of surface functional groups present. Such an analysis was conducted, and is described subsequently. First, however, we consider sorption studies performed at different pHs, which provided further insight into the adsorption process.

Effect of pH on Zn[II] Sorption. Because the surface charge density for both pristine and O-MWCNTs has been previously determined to be negative at the pH of the sorption experiments (6.5−6.8),[32] it is reasonable to assume an electrostatic adsorption mechanism and a specific adsorption of Zn^{2+} with the negatively charged surface groups on the MWCNT surface. Thus, Zn[II] sorption depends on the quantity of negatively charged functional groups on the MWCNTs, and perhaps particularly on the quantity of the carboxyl groups that may represent the principal source of charge in the moderate pH range. In this regard, other investigators have previously discussed how cationic metal species may be specifically adsorbed by negatively charged carboxyl groups on activated carbons.[7,9,12]

In order to investigate the role of pH on the adsorption of Zn[II] by MWCNTs, Zn[II] sorption (q_e) was measured at pH

values between 2 and 7 using an initial concentration of Zn[II] ($[Zn[II]]_0$ = 2.9 mM) that led to high equilibrium Zn[II] concentrations (C_e > 0.8 mM). Results from these studies are shown in Figure S7 in the Supporting Information. The adsorbed mass of Zn[II] on each MWCNT increased as a function of pH. A substantial (roughly 3- to 4-fold) increase in Zn[II] sorption capacity was observed between pH 3 and 5 for all MWCNTs studied. By contrast, sorption changes were comparatively minor outside of this range; for example, q_e was steady to within ±15% for pH between 5 and 7. These results likely reflect the importance of carboxyl groups (pK_a 3−5), which likely deprotonated to their negative form as the pH was increased within this range. Subsequently, in this paper, we describe various sorption models that allow us to consider relative contributions of different site types to sorption. Interestingly, the q_e changes observed between pH 3 and 5 of Figure S7 in the Supporting Information agree reasonably well (always within a factor of 2 and often much better) with the amounts of sorption that our "best" model (eq 4a, discussed subsequently) would assume to be associated with carboxylic groups at $[Zn^{2+}]_{equil} \approx 2.5$ mmol/L, as relevant to Figure S7.

Effect of Carboxyl Groups on Zn[II] Sorption. To better understand the effect of carboxyl functional groups on Zn[II] sorption, we independently characterized 16 differently prepared O-MWCNT samples with respect to the quantity and distribution of oxygen-containing functional groups, as measured by XPS in conjunction with chemical derivatization. Results are given in Table 2. One-point sorption data at a fixed C_e value of Zn[II] at $C_e \cong 2.8$ mM were also obtained on these same samples in order to provide a measure of their sorption properties. The single-point approach was necessary because of the comparatively large quantity of O-MWCNTs required for both chemical derivatization (~50 mg) and sorption studies (~5 mg per sample). Using the results shown in Table 2, q_e/BET-SA values were plotted against the percentage of oxygen determined by XPS (Figure 4a) and against each individual type of surface functional group that could be assayed with chemical derivatization (hydroxyl, carbonyl, and carboxyl groups) (Figure 4b−d). Linear regression reveals that Zn[II] sorption capacity has a stronger correlation with carboxyl groups (r^2 = 0.79) than with total oxides (r^2 = 0.52) and a much stronger correlation than with hydroxyl groups (r^2 = 0.09) or carbonyl groups (r^2 = 0.13). For the correlation with carboxyl groups (Figure 4b), all Zn[II] sorption data lay in the 95% confidence interval line except for three minor outliers, two of which fall quite close to the interval lines. These are the three O-MWCNTs treated with H_2SO_4/HNO_3, including the H_2SO_4/HNO_3 sample treated in our laboratory, NL-H_2SO_4/HNO_3, and NL-$\mu\lambda/H_2SO_4/HNO_3$. However, analogous to the data shown in Figure 3, the nonzero y-intercepts in Figure 4b (0.37 μmol Zn[II]/m^2) reveal that carboxyl groups are not the only sites responsible for Zn[II] sorption.

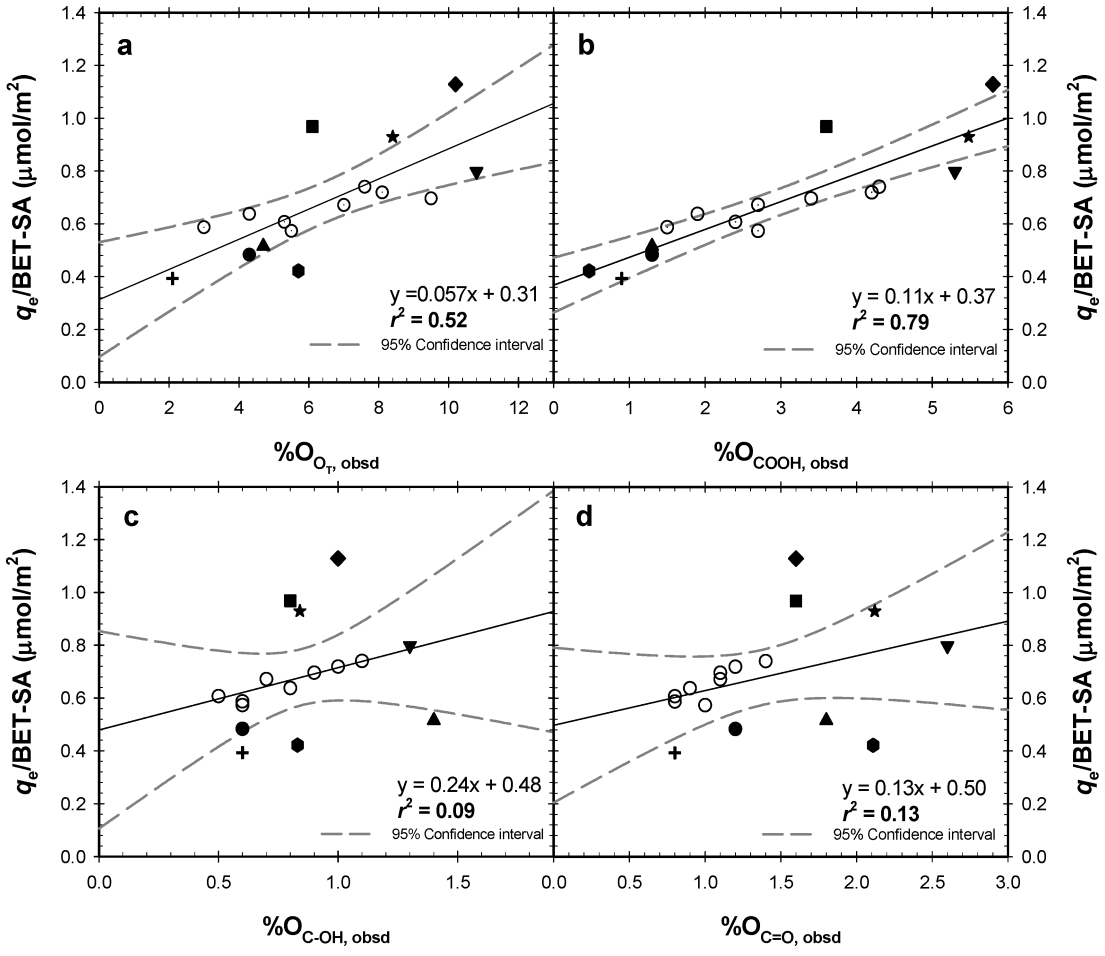

Figure 4. Surface area normalized sorption capacities (q_e/BET-SA) obtained for Zn[II] on pristine MWCNT and O-MWCNTs plotted against (a) total oxygen (O_{OT}), (b) carboxyl (O_{COOH}), (c) hydroxyl (O_{C-OH}), and (d) carbonyl ($O_{C=O}$). In all of these experiments, q_e/SA values are based on one point sorption isotherms obtained at $[Zn^{2+}]_e \cong 2.8$ mM, I = 0.01 M. In all figures, the cross symbols represent pristine MWCNTs, the open symbols represent MWCNTs oxidized with HNO_3, and the solid symbols represent the non-HNO_3-treated samples. Note: Symbols for materials are shown in Table 2.

Table 3. Sorbed Zn[II] Concentration at $C_e \cong 2.8$ mM and Site Distributions of Surface Carbon for MWCNTs That Had Been Oxidized to Varying Extents

treatment		$q_{e,2.8}$/BET-SA (μmol/m^2)[a]	$\%C_{O_T}$[b]	$\%C_{COOH}$[b]	$\%C_{C-OH}$[b]	$\%C_{C=O}$[b]	$\%C_{residual}$[b]	$\%C_{graphene}$[b]
pristine	+	0.40	5.2	1.5	1.8	2.6	−0.6	94.8
10%-HNO_3	○	0.59	7.2	2.4	1.9	2.5	0.4	92.8
20%-HNO_3	○	0.64	10.8	3.1	2.7	3.0	1.9	89.2
30%-HNO_3	○	0.61	13.3	3.9	1.8	2.7	4.9	86.7
40%-HNO_3	○	0.57	13.7	4.4	2.1	3.1	4.2	86.3
50%-HNO_3	○	0.72	20.1	7.2	3.7	4.9	4.5	79.9
60%-HNO_3	○	0.74	18.3	7.0	3.2	4.0	4.2	81.7
70%-HNO_3-a	○	0.70	26.5	5.8	2.9	3.9	13.9	73.5
70%-HNO_3-b	○	0.67	18.7	4.5	2.3	3.6	8.3	81.3
70%-HNO_3-b_ F[c]	●	0.48	11.8	2.1	1.9	3.9	3.9	88.2
H_2SO_4/HNO_3	♦	1.13	25.1	10.0	3.4	5.5	6.2	74.9
NL-H_2SO_4/HNO_3	■	0.95	14.1	5.9	2.5	5.4	0.3	85.9
NL-$\mu\lambda/H_2SO_4/HNO_3$	▼	0.80	28.1	9.2	4.6	8.9	5.4	71.9
NL-$\mu\lambda/H_2SO_4/HNO_3$_F[c]	▲	0.52	13.1	2.2	4.5	5.8	0.7	86.9
$KMnO_4$	★	0.71	19.1	9.2	2.8	7.1	−0.1	80.9
$KMnO_4$_F[c]	⬢	0.32	18.0	0.8	2.7	6.9	7.5	82.0

[a] Adsorbed Zn[II] on the MWCNTs at $[Zn[II]]_e \cong 2.8$ mM, $I = 0.01$ M, pH = 6.5−6.8. Shown are the average values based on three replicates. [b] The % of surface carbon associated with oxygen and with specific oxygen groups of different types was estimated from the total surface oxygen percentage and the functional group distribution data reported in Table 1, using methods described in Appendix I of the Supporting Information. $\%C_{Graphene}$ is estimated from these results and the XPS data for total % surface carbon. See the Supporting Information for details. [c] Samples ending with "_F" were furnace-treated under argon at 400 °C.

Table 4. Correlation of Sorbed Zn[II] Concentration at $C_e \cong 2.8$ mM with %C Associated with Various Surface Functional Groups

	correlations	F value[a]	r^2
a	$[q_{e,2.8}/\text{BET-SA}, \mu\text{mol/m}^2] = 0.0038[\%C_{graphene}] + 0.022[\%C_{OT}]$	0.029	0.29
b	$[q_{e,2.8}/\text{BET-SA}, \mu\text{mol/m}^2] = 0.0041[\%C_{graphene}] + 0.068[\%C_{COOH}]$	0.0086	0.79
c	$[q_{e,2.8}/\text{BET-SA}, \mu\text{mol/m}^2] = 0.0042[\%C_{graphene}] + 0.069[\%C_{COOH}] + 0.0015\{[\%C_{C-OH}] + [\%C_{C=O}] + [\%C_{residual}]\}$	0.011	0.74
d	$[q_{e,2.8}/\text{BET-SA}, \mu\text{mol/m}^2] = 0.0045[\%C_{graphene}] + 0.070[\%C_{COOH}] - 0.028[\%C_{C-OH}] + 0.0074[\%C_{C=O}] - 0.00047[\%C_{residual}]$	0.0089	0.77

[a] F value $= 1/\nu\Sigma[\text{observed } q_{e,2.8}/\text{BET-SA} - \text{calculated } q_{e,2.8}/\text{BET-SA}]^2$, where ν is the number of degrees of freedom.

Effect of Graphenic Carbon on Zn[II] Sorption. Other researchers[9,11,12] have studied the adsorption of heavy metal ions on activated carbons with different chemical compositions. They have suggested that although adsorption is strongest on carboxyl and lactone groups, sorption likely also occurs due to metal interactions with π-electrons in the graphene layer. These previous studies suggest that graphenic C atoms exhibit a basic character which allows them to serve as sorption sites for positively charged hydrated metal cations in aqueous solutions.[50]

To clarify the role of graphene-like carbon groups on Zn[II] sorption with MWCNTs, we have calculated the fractional concentration of graphene-like carbon atoms at the MWCNT surface, assuming that carbon atoms could be considered as being either surface oxides or graphenic carbon. Taking advantage of the well-defined structure of CNTs and assuming that oxidation was restricted to the surface, we estimated the relative fraction of surface carbon atoms that were graphenic and the fraction of surface carbon atoms that were associated with each of three types of oxygen-containing functional groups (i.e., carboxyl, carbonyl, and hydroxyl); see Appendix I in the Supporting Information for details. Results are shown in Table 3, where $\%C_{residual}$ represents the percent of surface carbon atoms associated with oxygen-containing functional groups other than those that cannot be quantified using chemical derivatization, that is, groups other than hydroxyl, carbonyl, and carboxylates, such as ethers and esters (see Experimental Section). We considered the relative surface-site densities given in Table 3 in order to better understand their roles on Zn[II] sorption properties onto O-MWCNTs. Note that Table 3 shows the fraction of carbon associated with oxygen-containing functional groups and graphenic-carbon atoms (i.e., on a surface carbon basis), whereas Table 2 provides the quantity and distribution of oxygen-containing functional groups based on percent of oxygen atoms.

Using the relative surface-site densities of C atoms in Table 3 for each O-MWCNT, we have compared the experimentally measured q_e/BET-SA values (at $C_e \cong 2.8$ mM) of 16 MWCNTs (shown in Table 3) against values that are calculated using a fitted model which assumes that the total q_e/BET-SA value is the sum of independent contributions from different types of surface carbon. For example, in this analysis, the percent contribution from graphenic carbon to the sorption capacity of each O-MWCNT is given by the product of $\%C_{graphene}$ and the appropriate best-fit coefficient, which will correspond to $(q_e/SA)_{graphene}$ based on the multisite Langmuir adsorption isotherm described in eq 1. Results are shown in Table 4 and Figure 5. The panels of Figure 5 contain plots of observed q_e/BET-SA values against model-calculated q_e/BET-SA values using various models of surface site contribution to sorption. Based on F values ($= 1/v\sum[\text{observed } q_e - \text{calculated } q_e]^2$, where v is the number of degrees of freedom) and r^2 values, the best-fit regression was found to be correlation (b) in Table 4 and Figure 5, that is, the correlation based on the assumption that sorption can be modeled using only the graphenic and carboxyl content ($q_{e,2.8}/\text{BET-SA} = a[\%C_{graphene}] + b[\%C_{COOH}]$). By contrast, model (a), which uses graphenic-carbon atoms and all carbon atoms associated with surface oxygen ($q_{e,2.8}/\text{BET-SA} = 0.0038[\%C_{graphene}] + 0.022[\%C_{Ototal}]$), provided a relatively poor fit of observed results. Predictions using model (a) were especially poor for the three thermally annealed MWCNTs, which deviated significantly from the 95% confidence interval (Figure 5a and Table 4). For the best-fit correlation (corresponding to (b) in Table 4 and Figure 5), most of the experimental data were well predicted by the regression, including the three thermally annealed samples; however, data

(50) Dougherty, D. A. *Science* **1996**, *271*, 163.

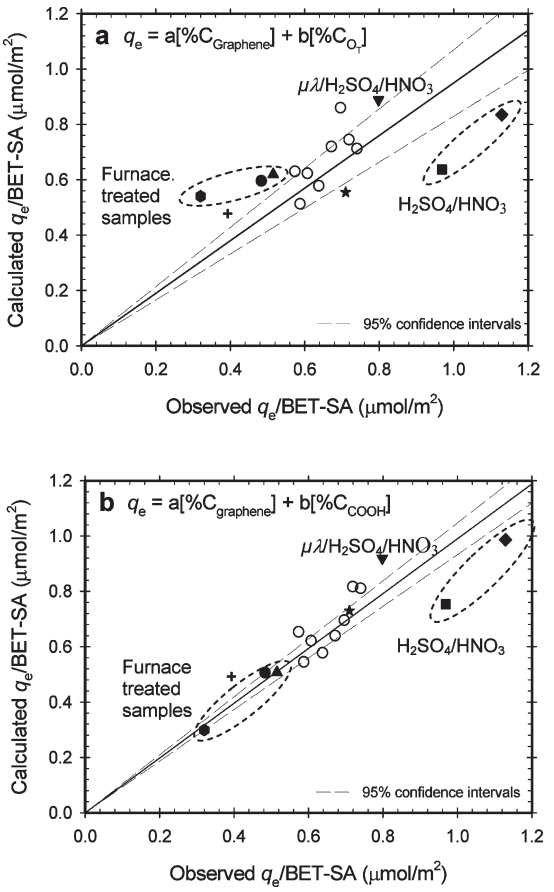

Figure 5. Correlation between experimentally determined q_e/BET-SA versus calculated q_e/BET-SA by linear regression using (a) the percent site of graphenic groups and surface carbon atoms bound to oxygen and (b) the percent of graphenic surface carbon atoms and surface bound carboxyl groups. Experimentally determined q_e/BET-SA values were obtained using $[Zn^{2+}]_e \cong 2.8$ mM, $I = 0.01$ M. In both figures, the cross symbol represents pristine MWCNT and open circle symbols represent MWCNTs oxidized with HNO_3. Solid symbols represent non-HNO_3-treated samples. Note: Symbols for the samples are shown in Table 3.

for a few MWCNTs (including the three O-MWCNT samples treated by H_2SO_4/HNO_3) still fell outside of the 95% confidence intervals.

Note from the data in Table 3 that the principal effect of the furnace treatment was to remove COOH groups; all three furnace-treated O-MWCNTs still contained substantial fractions of C═O surface sites, and for the $KMnO_4$_F MWCNTs the fraction of "residual" (unidentified) oxygen functional groups rose substantially after treatment. In terms of the results reported in Table 4 and Figure 5a, we believe that the poor regression for annealed O-MWCNTs was because this correlation considered the total oxygen content, yet it is only the carboxyl groups that contributed significantly to Zn[II] sorption. In other words, the largely decarboxlyated furnace-treated tubes having oxygen-containing functional groups other than −COOH that did not contribute significantly to sorption. In this regard, note that after furnace treatment the measured fraction of carboxylated surface carbon for O-MWCNTs treated with $KMnO_4$ decreased from 9.2% to 0.8% although the total oxygen content remained high (19.1% vs 18.0% before treatment; see Table 3).

In terms of this overall best-fit regression (regression (b) of Table 4), the coefficient for $\%C_{COOH}$ (= 0.068), which corresponds to $(q_e/SA)_{COOH}$ in the multisite Langmuir isotherm, is roughly 17 times higher than the coefficient for $\%C_{graphene}$ (= 0041), which corresponds to $(q_e/SA)_{graphene}$ (Figure 5b and Table 4). This result reveals that Zn[II] sorption to the COOH sites was collectively much stronger than that to graphenic carbon. This is largely a reflection of the fact that the carboxyl groups were deprotonated in our sorption experiments (pH ≈ 6) and were therefore able to exhibit a strong affinity for divalent metal cations. Nonetheless, graphenic-carbon atoms still contributed substantially to the total sorption capacity owing to their relatively high surface site density in MWCNTs.

Finally, we note that the regression (d) of Table 4 also provided an excellent fit to the data, similar to that of regression (b) in Figure 5. Note, however, that the coefficients of the hydroxyl and "residual" groups were negative (with large uncertainties) in this case, such that the contribution from these groups served to simply negate the regressed contribution of the carboxyl. We believe that the success of this regression was simply an artifact of the regression process and not reflective of any physicochemical process.

Langmuir Two-Site Model. On the basis of results obtained from sorption data at fixed C_e, it is reasonable to hypothesize that the full sorption isotherm of Zn[II] to MWCNTs might also be well-described by a simple two-site Langmuir model;[51] Sposito has noted that two-site model fits are not necessarily mechanistic unless specific individual sites can be independently identified and characterized.[51] In the present study, we address this concern by means of independent measurement of the distribution of surface functional groups on the MWCNTs. A remaining concern, however, is that multiple "types" of COOH sites are likely to exist, owing to variations in the local chemical environment, for example, as associated with variability in relative proximity of COOH groups, and thus in the number of groups participating in sorption. Despite this remaining concern, it is useful to consider a "lumped" model for the COOH sites, which will be accurate so long as the relative *distribution* of "COOH-site types" does not change substantially among our different O-MWCNTs.

To explore this hypothesis, the Langmuir isotherm model (eq 1) was used with $n = 2$ to account for both of the two identified types of "lumped" and independent binding sites, that is, for graphenic-carbon and carboxyl groups:[11,51]

$$\frac{q_e}{SA} = \frac{1}{SA}\left(q_{e,\,graphene} + q_{e,\,COOH}\right)$$
$$= \frac{1}{SA}\left(\frac{q_{max\,,\,graphene} K_{L,\,graphene} C_e}{(1 + K_{L,\,graphene} C_e)} + \frac{q_{max\,,\,COOH} K_{L,\,COOH} C_e}{(1 + K_{L,\,COOH} C_e)}\right) \quad (2)$$

where $q_{max,graphene}$ and $q_{max,COOH}$, and $K_{L,graphene}$ and $K_{L,COOH}$ are the maximum adsorption capacities and the adsorption affinities for graphenic-carbon and carboxyl groups on the MWCNTs, respectively.

We conducted our analysis by considering fits of eq 2 to Zn[II] sorption isotherms obtained with four individual MWCNTs for which we had both the oxygen functional group distribution (Table 3) and multiconcentration isotherm data (Table 1). The four MWCNTs considered were P-MWCNTs (commercially obtained) and three O-MWCNTs, one of which was made in our laboratories (O-MWCNTs oxidized with H_2SO_4/HNO_3) and two of which were obtained from a commercial supplier (NL-$H_2SO_4/HNO_3$and NL-$\mu\lambda/H_2SO_4/HNO_3$). Individual fits to the four isotherms were obtained using all four fitting parameters of the Langmuir two-site model (eq 2) to minimize the sum of squared errors. As expected for a four-parameter model, the fits

(51) Sposito, G. *Soil Sci. Soc. Am. J.* **1982**, *46*, 1147.

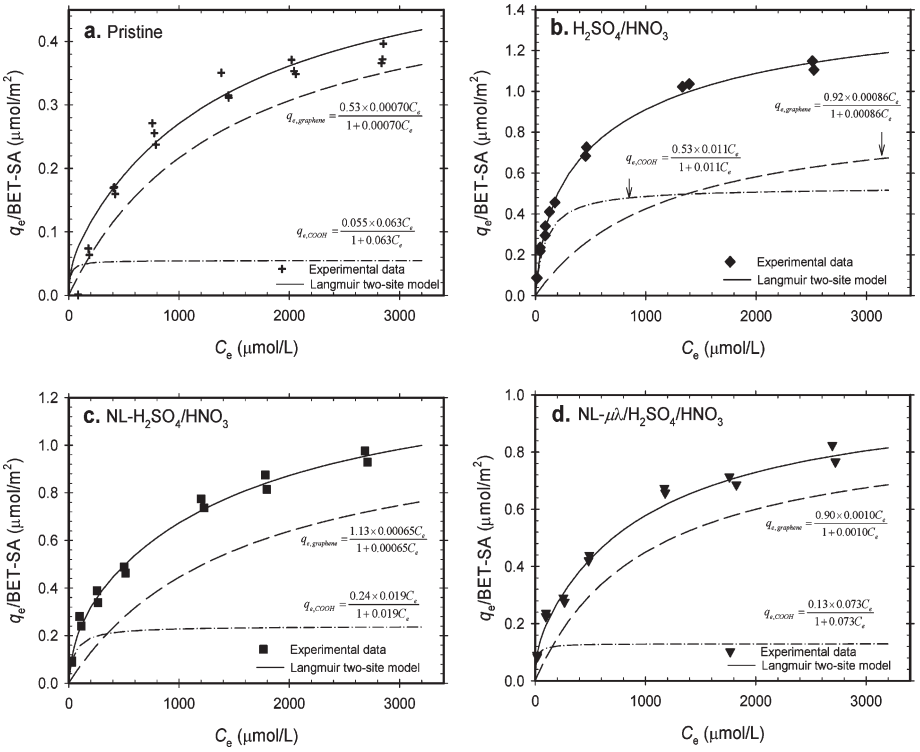

Figure 6. Fits of Zn[II] sorption isotherms using the Langmuir two-site model (eq 2) and individually fit parameter values for (a) P-MWCNTs, (b) O-MWCNTs oxidized with H_2SO_4/HNO_3, (c) O-MWCNTs oxidized with NL-H_2SO_4/HNO_3, and (d) O-MWCNTs oxidized with NL-$\mu\lambda/H_2SO_4/HNO_3$. The parameter values used for model simulation are shown in Table 5.

Table 5. Parameters for Langmuir Two-Site Isotherm Equation Based on Model Fitting to Zn[II] Sorption Data

sorbent			individually fit parameters (used for Figure 6)				calculated quantities		
treatment	[%$C_{graphene}$]	[%C_{COOH}]	$q_{max,graphene}$/BET-SA (μmol/m²)	$q_{max,COOH}$/BET-SA (μmol/m²)	$K_{L,graphene}$ (L/μmol)	$K_{L,COOH}$ (L/μmol)	α (μmol/m² per %$C_{graphene}$)[a]	β (μmol/m² per %C_{COOH})[a]	r^2
pristine	94.8	1.5	0.53	0.055	0.00070	0.063	0.0056	0.037	0.99
H_2SO_4/HNO_3	74.9	10.0	0.92	0.53	0.00086	0.011	0.012	0.053	0.99
NL-H_2SO_4/HNO_3	85.9	5.9	1.13	0.24	0.00065	0.019	0.013	0.041	0.99
NL-$\mu\lambda/H_2SO_4/HNO_3$	71.9	9.2	0.90	0.13	0.0010	0.073	0.013	0.014	0.99

sorbent			individually fit parameters (used for Figure 7)		common parameters (used for Figure 7)		calculated quantities		
treatment	[%$C_{graphene}$]	[%C_{COOH}]	$q_{max,graphene}$/BET-SA (μmol/m²)	$q_{max,COOH}$/BET-SA (μmol/m²)	$K_{L,graphene}$ (L/μmol)	$K_{L,COOH}$ (L/μmol)	α (μmol/m² per %$C_{graphene}$)[a]	β (μmol/m² per %C_{COOH})[a]	r^2
pristine	94.8	1.5	0.56	0.011	0.00090	0.023	0.0059	0.0073	0.99
H_2SO_4/HNO_3	74.9	10.0	1.22	0.35			0.016	0.035	0.99
NL-H_2SO_4/HNO_3	85.9	5.9	1.10	0.18			0.013	0.031	0.99
NL-$\mu\lambda/H_2SO_4/HNO_3$	71.9	9.2	0.77	0.23			0.011	0.025	0.99

[a] $q_{max,graphene}$/BET-SA = α[%$C_{graphene}$], $q_{max,COOH}$/BET-SA = β[%C_{COOH}]; see eq 3a for details.

are quite good (Figure 6). Linearization of the data allows a better comparison of the two-site and one-site models with respect to their ability to simulate the low concentration data; see Figure S8 in the Supporting Information. Such comparison reveals that the two-site model does a much better job than the one-site model at capturing both low- and high-concentration data. The results (Figure 6 and top half of Table 5) confirm that adsorption with graphenic-carbon sites is weaker than that with carboxyl sites. Encouragingly, the fitted K_L values fall within the same order of magnitude for three of the four materials ($K_{L,graphene}$ = 0.00070−0.0010 L/μmol and $K_{L,COOH}$ = 0.011−0.073 L/μmol, respectively; see Table 5). Note that NL-$\mu\lambda/H_2SO_4/HNO_3$ has the highest $K_{L,graphene}$ and $K_{L,COOH}$ values (Table 5, top) and sorption was also overpredicted by the regression shown in Figure 5b. As previously noted, Raman results (Figure S5 in the Supporting Information) suggest that this microwave-treated sample also has a significantly different I_D/I_G ratio compared to other O-MWCNTs.

In the modeling results discussed above (Figure 6), we used a total of four parameters to fit each isotherm, that is, 16 parameters to fit four data sets. To further explore the hypothesis that a single set of site energies can be used to understand all four materials, we re-evaluated the data using eq 2, but with an assumption of common $K_{L,graphene}$ and $K_{L,COOH}$ values for all four sorption isotherms, using values obtained by applying a search algorithm that minimized squared error for all four isotherms simultaneously. These results are shown in the bottom half of Table 5 and in Figure 7. The data fits are reasonably good,

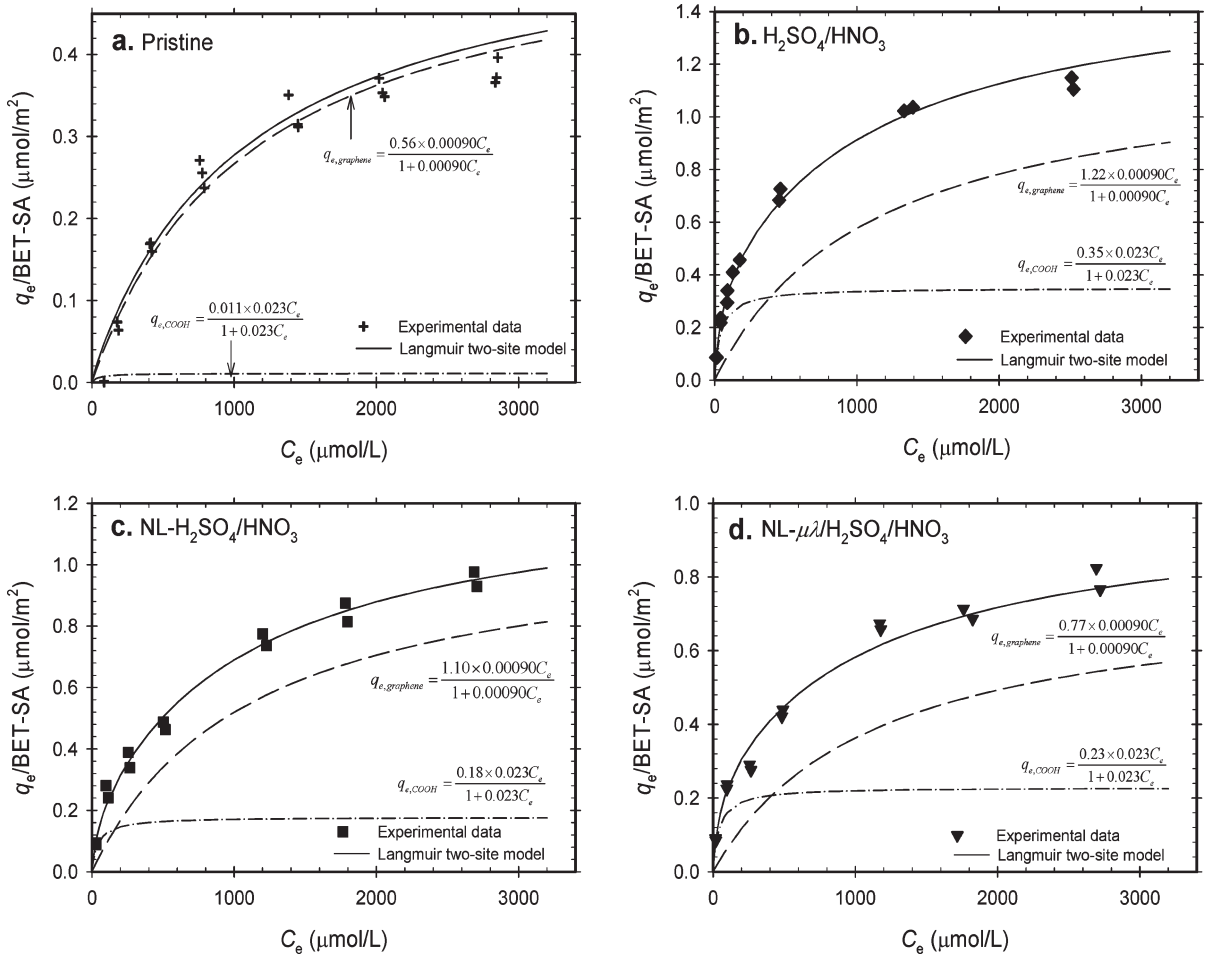

Figure 7. Fits of Zn[II] sorption isotherms using the Langmuir two-site model (eq 2 and two common parameters ($K_{L,graphene}$ and $K_{L,COOH}$) for (a) P-MWCNTs, (b) O-MWCNTs oxidized with H_2SO_4/HNO_3, (c) O-MWCNTs oxidized with NL-H_2SO_4/HNO_3, and (d) O-MWCNTs oxidized with NL-$\mu\lambda/H_2SO_4/HNO_3$. The parameter values used for model simulation are shown in Table 5.

confirming similar energetics of sorption for the two-site model with these four MWCNTs and suggesting that $K_{L,COOH}$ is ~26 times higher than $K_{L,graphene}$.

Finally, we explored the hypothesis that $q_{max,graphene}$ and $q_{max,COOH}$ values can be quantitatively predicted from independently determined BET-SA data and %C data (Table 3). To develop such a relationship, consider regression (b) in Table 4: $q_{e,2.8} = a[\%C_{graphene}] + b[\%C_{COOH}]$. By analogy, it is also reasonable to assume that $q_{max,graphene} = a_{max}[\%C_{graphene}]$ and $q_{max,COOH} = b_{max}[\%C_{COOH}]$. With this assumption, and recognizing that q_{max} occurs at $C_e = \infty$, we can use the fact that [$q_{e,max} = q_{e,graphene,max} + q_{e,COOH,max}$] to obtain the following relationships:

$$\frac{q_{e,max}}{SA} = \frac{1}{SA}\left(a_{max}\%C_{graphene} + b_{max}\%C_{COOH}\right) \qquad (3a)$$

or

$$\frac{q_{e,max}}{SA} = \alpha\%C_{graphene} + \beta\%C_{COOH} \qquad (3b)$$

where α represents a constant coefficient of proportionality between ($q_{max,graphene}$/BET-SA and [$\%C_{graphene}$] and β represents a constant coefficient of proportionally between $q_{max,COOH}$/BET-SA and [$\%C_{COOH}$]. Use of eqs 2 and 3b reduces the total number of fitting parameters down to four: $K_{L,graphene}$, $K_{L,COOH}$, α, and β. Application of this approach to our data set (i.e., applying only four adjustable parameters toward the simultaneous fit of all four of our complex data sets) led to the results shown in the Supporting Information, Figure S9 and Table S2. These results show that, although the approach provided good prediction for the P-MWCNTs, there was substantial over-prediction for NL-$\mu\lambda/H_2SO_4/HNO_3$ and under-prediction for the two H_2SO_4/HNO_3-treated samples.

As previously noted, the Raman data had suggested significant differences for the NL-$\mu\lambda/H_2SO_4/HNO_3$ material (Figure S5 in the Supporting Information), with I_D/I_G ratios that may imply less structural damage than for other O-MWCNTs and also less loss of surface area after oxidation. Under the assumption that carboxylate and graphenic surface chemistry may be somehow different for this sample, we reconducted the "common-fit" analysis using only the other three MWCNTs. These results are shown in Figure 8. Reasonably good fits were found for all three materials, seeming to confirm our hypothesis that NL-$\mu\lambda/H_2SO_4/HNO_3$ was an anomalous sample, in that the sorption properties of the remaining three MWCNTs can be described by a single two-site model. In other words, common values of α and β seem to exist for the three other materials but not for NL-$\mu\lambda/H_2SO_4/HNO_3$.

The $K_{L,graphene}$ and $K_{L,COOH}$ values associated with Figure 8 and Table 6 are 0.00026 and 0.0061 L/μmol, respectively, suggesting that, on a per-carbon-atom basis, COOH groups are roughly 24 times more energetic than the unmodified graphenic-carbon groups in terms of Zn[II] sorption. This result is similar to that obtained previously from the fits of Figure 7. The final model used

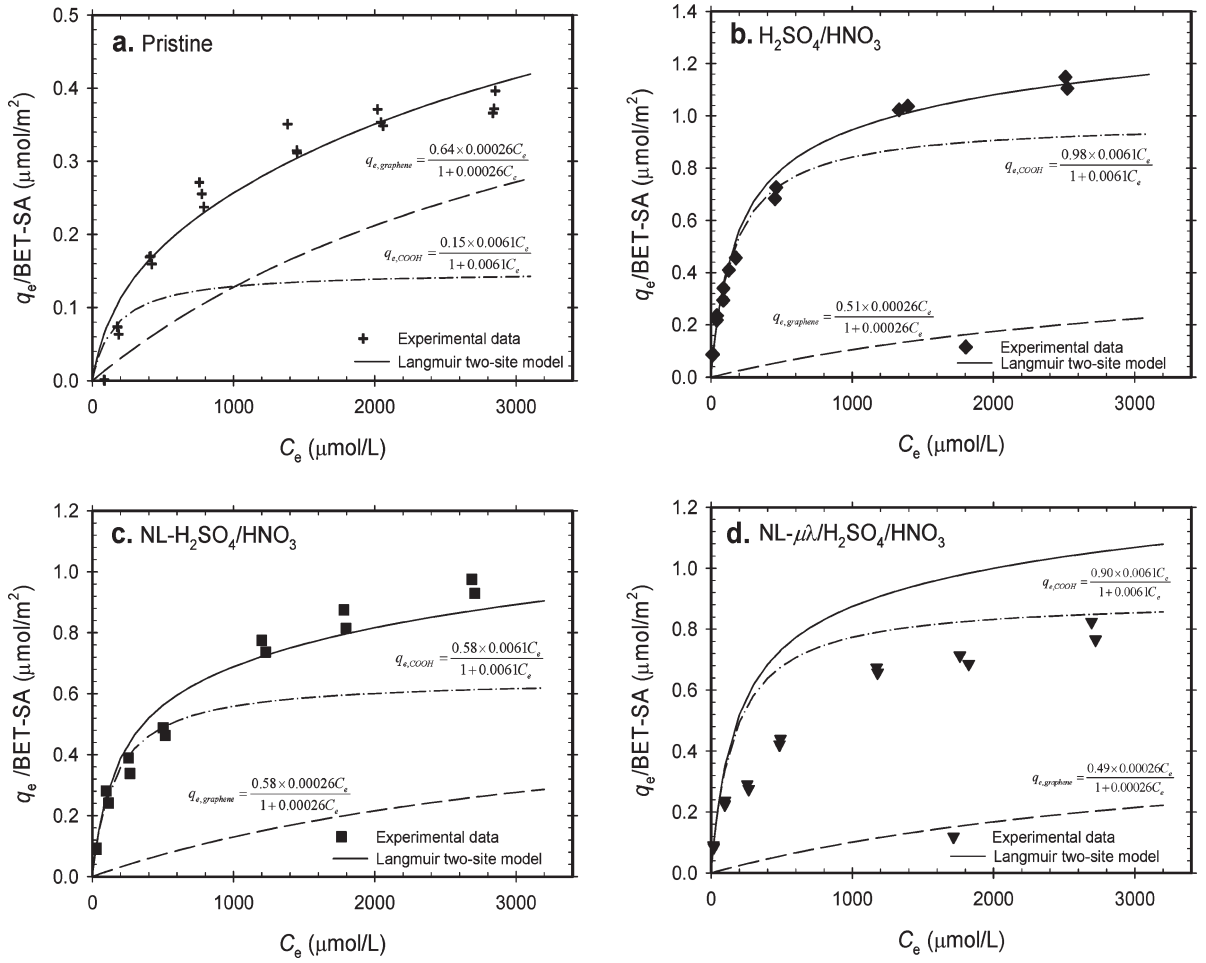

Figure 8. Recalculated common parameter ($K_{L,graphene}$ and $K_{L,COOH}$) fits for the data shown in Figure 7 using the Langmuir two-site model (eq 2) for (a) P-MWCNTs, (b) O-MWCNTs oxidized with H_2SO_4/HNO_3, (c) O-MWCNTs oxidized with NL-H_2SO_4/HNO_3, and (d) O-MWCNTs oxidized with NL-$\mu\lambda/H_2SO_4/HNO_3$. Note: Values for common parameters are shown in Table 6 and are also used for the model simulations of NL-$\mu\lambda/H_2SO_4/HNO_3$ in panel (d). The NL-$\mu\lambda/H_2SO_4/HNO_3$ sample is anomalous in several regards; see text for details.

Table 6. Common Parameters for Langmuir Two-Site Isotherm Equation Based on Model Fitting to Observed Zn[II] Sorption Data but with Exclusion of Data from NL-$\mu\lambda/H_2SO_4/HNO_3$ in the Search for Common Parameters

sorbent			common parameters (used for Figure 8)[a]				calculated quantities		
treatment	[%$C_{graphene}$]	[%C_{COOH}]	$K_{L,graphene}$ (L/μmol)	$K_{L,COOH}$ (L/μmol)	α (μmol/m^2 per %$C_{graphene}$)[b]	β (μmol/m^2 per %C_{COOH})[b]	$q_{max,graphene}$/BET-SA (μmol/m^2)	$q_{max,COOH}$/BET-SA (μmol/m^2)	r^2
pristine	94.8	1.5	0.00026	0.0061	0.0068	0.098	0.64	0.15	0.99
H_2SO_4/HNO_3	74.9	10.0					0.51	0.98	0.99
NL-H_2SO_4/HNO_3	85.9	5.9					0.58	0.58	0.98
NL-$\mu\lambda/H_2SO_4/HNO_3$	71.9	9.2					0.49	0.90	0.93

[a] Common α, β, $K_{L,graphene}$, and $K_{L,COOH}$ values were obtained from the minimization using a sum of relative squared errors but without including data from NL-$\mu\lambda/H_2SO_4/HNO_3$. [b] $q_{max,graphene}$/BET-SA = α[%$C_{graphene}$], $q_{max,COOH}$/BET-SA = β[%C_{COOH}]; see eq 3b for details.

for all four panels of Figure 8 is given by eq 4b below:

$$\frac{q_e}{SA} = \left(\frac{\alpha[\%C_{graphene}]K_{L,graphene}C_e}{(1+K_{L,graphene}C_e)} + \frac{\beta[\%C_{COOH}]K_{L,COOH}C_e}{(1+K_{L,COOH}C_e)}\right) \quad (4a)$$

$$\frac{q_e}{SA}\left[\frac{\mu mol\ Zn^{2+}}{m^2}\right] = \left(\frac{0.0068[\%C_{graphene}]0.00026C_e}{(1+0.00026C_e)} + \frac{0.098[\%C_{COOH}]0.0061C_e}{(1+0.0061C_e)}\right) \quad (4b)$$

where C_e is the equilibrium Zn^{2+} concentration in μmol/L as previously noted.

In order to better understand our confidence in the estimated values of our four parameters ($K_{L,graphene}$, $K_{L,COOH}$, α, and β) for use with the three fitted isotherms, we conducted a sensitivity analysis on the goodness of fit, as measured by the sum of squared errors from all three isotherms. Results are given in Figure S10 of the Supporting Information. These results indicate that only a 15% increase in the sum of squared errors is obtained using values of these four parameters as follows: $K_{L,graphene}$, 0.00020−0.00033; $K_{L,COOH}$, 0.0052−0.0071; α, 0.0054−0.0083; and β, 0.088−0.107. These ranges provide an initial estimate of

uncertainty for these parameters, as applied to the three materials tested.

Of course, actual uncertainties are much higher for materials other than the three to which eq 4 was fit. One important uncertainty is the assumed proportionality of q_e to BET-SA as implied by the normalized quantity on the left-hand side. This assumption was made for purposes of discussion but has not yet been rigorously tested. Other uncertainties relate to the lumping of multiple site types into two, as previously discussed. Clearly, one should not expect eq 4 to hold widely for carbonaceous materials, or even for all MWCNTs. This has been illustrated by the results for NL-$\mu\lambda$/H_2SO_4/HNO_3, in Figure 8d. Equation 4 will also not be accurate for highly complex and microporous materials (such as NC1 and GAC), where site heterogeneity will be even more important. Therefore, application of our multisite Langmuir sorption modeling is not deemed appropriate for these materials. For well characterized materials such as MWCNTs, however, we believe that this general modeling approach has the potential to be reasonaly accurate, as suggested by Figure 8a−c. As noted above, further testing is required, however, with a larger set of O-MWCNTs.

4. Conclusions

Sorption properties of MWCNTs toward Zn[II] and Cd[II] were measured for both pristine and oxidized materials. Maximum adsorption capacities obtained for O-MWCNTs were found to be slightly higher than those of activated carbon (AC) when normalized to surface area, even though the O-MWCNTs had less surface oxygen content. On the other hand, surface-normalized maximum adsorption capacities for a natural char (NC1) were much higher than those for O-MWCNTs, consistent with the much higher oxygen content of the char material. In addition, Zn[II] demonstrated stronger sorption than Cd[II] for all materials studied, although increasing surface oxidation had more effect on the sorption of Cd[II] than on the sorption of Zn[II]. The latter finding implies that the relative importance of oxygen-containing functional groups is greater for cadmium than for zinc.

Investigations of sorption isotherms using a suite of well-characterized O-MWCNTs provided specific information about the role of various surface oxides. A strong linear correlation was observed between maximum sorption capacity and surface oxygen concentration but with a strong nonzero intercept (Figure 3). This intercept revealed that graphenic carbon must also be contributing to sorption.

Independent estimates of site densities for three oxygen functional groups (hydroxyl, carbonyl, and carboxyl groups) and graphenic carbon on 16 MWCNT materials were used in combination with single-concentration Zn[II] sorption data to confirm the importance of the graphenic sites. In addition, correlations of these sorption data with the site densities of different oxygen functional groups revealed that only the COOH-carbon and graphenic-carbon sites were contributing substantially to sorption.

For the four MWCNTs for which we had both functional group distributions and full isotherm data (i.e., P-MWCNTs and three types of O-MWCNTs), excellent isotherm fits were obtained using a two-site Langmuir isotherm model that considered only the graphenic and carboxyl carbon groups. Model fits were obtained using both individual and common parameter assumptions. The results suggest that all four materials have common $K_{L,graphene}$ and $K_{L,COOH}$ values, with the latter being roughly 25 times higher than the former. Values of α [$= q_{max,graphene}/(\text{BET-SA})(\%C_{graphene})$] and β [$= q_{max,COOH}/(\text{BET-SA})(\%C_{COOH})$] for three of the four materials were also reasonably similar, with final best estimates as given in Table 6. Causes of lower than expected observations of q_{max} in the fourth material (a commercial microwave-treated material) are unknown, but Raman spectroscopy suggested a difference in the structure of these MWCNTs. The series of regression results imply that the distribution of COOH sites is different for NL-$\mu\lambda$/H_2SO_4/HNO_3 than that in the other three samples, and that these differences affected α and β more strongly than $K_{L,graphene}$ and $K_{L,COOH}$.

Overall, our results provide important new information about Langmuir sorption affinity and capacity for the adsorption of metal cations by MWCNTs and O-MWCNTs from aqueous solution, including an improved understanding of the importance of surface chemistry and different oxidative treatments. Further study with other treated samples is needed to confirm our proposed approach for estimating q_{max} as well as additional studies with other cations to investigate the applicability of these findings to other divalent cations and the nature of competition for sorption sites among different aqueous species.

Acknowledgment. The authors gratefully acknowledge financial support from the National Science Foundation (Grant No. BES0731147), the Environmental Protection Agency (Grant No. RD-83385701-0), and the Institute for Nanobiotechnology at Johns Hopkins University. We would also like to acknowledge Dr. Yo-Rhin Rhim (Department of Mechanical Engineering, Johns Hopkins University, Baltimore, MD) for collecting the Raman spectroscopy data. Additionally, we acknowledge the JHU Materials Science and Engineering Surface Analysis Laboratory for XPS analysis.

Supporting Information Available: Four appendices, which contain two tables and ten figures. Appendix I provides "Calculation of Surface Site Densities from XPS Data" and contains the following two figures: Figure S1, "Schematic representation of an O-MWCNT (shown along the central axis) with oxygen-containing functional groups decorating the outermost surface layer; and Figure S2, "Schematic of the O-MWCNT surface illustrating the definition of $O_{x(surface)}$ and $C_{x(surface)}$ where x is shown for COOH, C−OH, C=O, and graphene." Appendix II provides "Additional Tables to Support Manuscript Discussion, including Table S1, "List of carbonaceous materials and BET surface area"; and Table S2, "Common parameters for Langmuir two-site isotherm equation based on model fitting to observed Zn[II] sorption data (parameters as used for Figure S9)." Appendix III provides "Additional Figures to Support Manuscript Discussion," including Figure S3, "Kinetic experiments for Zn[II] sorption to pristine MWCNT, granular activated carbon (GAC-F400), and natural char (NC1); Figure S4, "Comparison of Zn[II] sorption isotherms with the same O-MWCNT (8% O) before and after dispersion in solution"; Figure S5, "Raman spectra (λ = 514.57 nm) of pristine and O-MWCNTs"; Figure S6, "Zn[II] and Cd[II] sorption isotherms for carbonaceous materials based on BET-surface area: (a) pristine MWCNT, natural char, and granular activated carbon, (b) pristine MWCNT and three different treated O-MWCNTs (53%-HNO_3-a, b, H_2SO_4/HNO_3, and NL-$\mu\lambda$/H_2SO_4/HNO_3); Figure S7, "Effect of pH on Zn[II] sorption capacities of pristine MWCNT and O-MWCNTs"; Figure S8, "Linearized fits of Zn(II) sorption isotherms for (a) P-MWCNTs, (b) O-MWCNTs oxidized

with H_2SO_4/HNO_3, (c) O-MWCNTs oxidized with NL-H_2SO_4/HNO_3, and (d) O-MWCNTs oxidized with NL-$\mu\lambda$/H_2SO_4/HNO_3, showing data fits with both the Langmuir one-site model and the Langmuir two-site model of Figure 6 and Table 5; Figure S9, "Zn[II] sorption isotherms for (a) pristine MWCNT, (b) O-MWCNTs oxidized with H_2SO_4/HNO_3, (c) O-MWCNTs oxidized with NL-H_2SO_4/HNO_3, and (d) O-MWCNTs oxidized with NL-$\mu\lambda$/H_2SO_4/HNO_3"; Figure S10, "Sensitivity test of $K_{L,Graphene}$, $K_{L,COOH}$, α, and β variables for the best fits (Figure 8 in the text) by the Langmuir two-site model. This material is available free of charge via the Internet at http://pubs.acs.org.